STABILITY OF ROOT REINFORCED STREAMBANKS: NUMERICAL MODELING AND LABORATORY EXPERIMENTS

By

RACHEL MICHELLE CANCIENNE

Bachelor of Science in Biosystems Engineering

Oklahoma State University

Stillwater, Oklahoma

2006

Submitted to the Faculty of the
Graduate College of
Oklahoma State University
in partial fulfillment of
the requirements for
the Degree of
MASTER OF SCIENCE
May, 2008

STABILITY OF ROOT REINFORCED STREAMBANKS:

NUMERICAL MODELING AND LABORATORY

EXPERIMENTS

Thesis Approved:

Dr. Garey A. Fox
Thesis Adviser

Dr. Glenn O. Brown

Dr. Michael D. Smolen

Dr. A. Gordon Emslie
Dean of the Graduate College

ACKNOWLEDGEMENTS

I would like to express my sincere gratitude to all faculty, staff, friends, and family who encouraged and challenged me throughout this educational experience. I would foremost like to thank Dr. Garey Fox, my graduate advisor, for his instruction and wisdom during the pursuit of this degree. His knowledge and support were instrumental in both my personal success and the achievements of this work. I would also like to thank Dr. Glenn Wilson, Dr. Andrew Simon, and Dr. Natasha Pollen-Bankhead of the USDA-ARS National Sedimentation Laboratory for their guidance on this research. Additionally, thank you to Dr. Glenn Brown and Dr. Michael Smolen for their excellent committee membership and editorial advice.

The laboratory experiments in this research would not have been possible without the support of my fellow graduate students. I would like to send my utmost gratitude to Maria Chu-Agor for being both an exceptional lab partner and a constant source of entertainment and gossip during our many summer hours packing and conducting soil block experiments. I would like to thank Dr. Onur Akay for aiding in the design of the three-dimensional blocks, as well as John Fuchs and Jorge Guzman for helping haul seemingly endless quantities of soil to the lab and greenhouse.

Finally, I would like to thank all that inspire me on a daily basis. Thank you to my family and friends for their unconditional support. Thank you to my parents for all of the encouragement and opportunities which they have provided in my life. I would also like to thank Jana Moore for her guidance throughout my years at OSU and all of the faculty and staff of the Biosystems and Agricultural Engineering Department.

TABLE OF CONTENTS

Chapter Page

LIST OF TABLES

Table Page

LIST OF FIGURES

Figure Page

Figure Page

Figure Page

CHAPTER I

INTRODUCTION

Sediment is a primary pollutant worldwide and in many watersheds the majority (up to 85%) of this sediment originates from streambanks (Bull and Kirkby, 1997; Simon ***et al.***, 2000; Evans ***et al.***, 2006). Sediment can affect stream flow regimes, chemical transport, and natural phenomena downstream from an eroded site; therefore, controlling this sediment loading could play a key role in the protection and preservation of both human and freshwater ecosystem health.

1.1 Seepage Erosion

Though there are many mechanisms that lead to streambank instability (i.e., toe erosion by streamflow undercutting and removal of negative pore-water pressure via precipitation infiltration), subsurface seepage erosion has recently been highlighted as an important contributing factor to streambank sediment loss and streambank failure (Fox ***et al.***, 2007c). High infiltration rates can lead to the development of shallow perched water tables above less-permeable soil layers, causing large hydraulic gradients and rapid subsurface flow toward stream channels (Coates, 1990; Wilson ***et al.***, 1991; Jones, 1997; Fox ***et al.***, 2006) or between layers with contrasting hydraulic

conductivity (Hagerty, 1991a, 1991b), as depicted in Figure 1-1. This subsurface flow results in additional forces on bank sediment and can cause the liquefaction of soil particles which seep out of the bank face, eroding and undercutting the bank material and depositing sediment into the underlying stream (Higgins, 1982; Higgins, 1984; McLane, 1984; Dunne, 1990; Fox ***et al.***, 2007a, 2007b, 2007c).

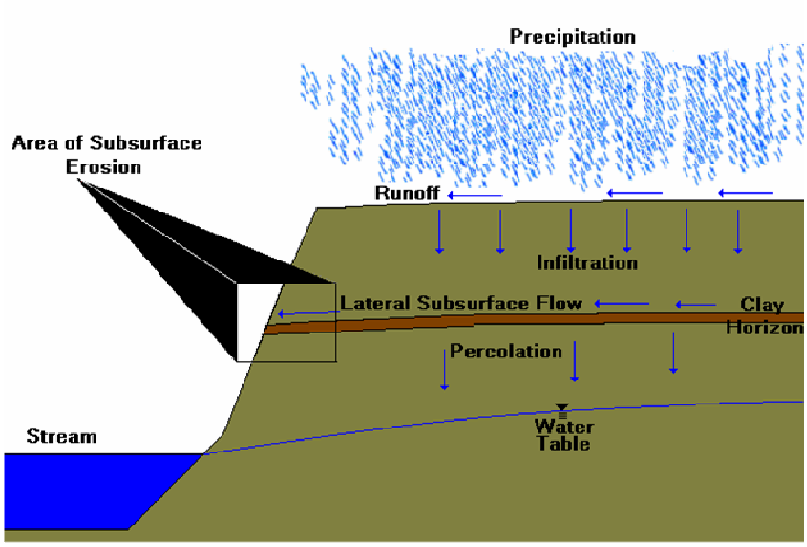

Figure 1-1. Illustration of subsurface flow erosion of infiltrated water flowing in perched water tables in riparian zones (Fox *et al.*, 2006).

In recent work to highlight the importance of undercutting due to seepage erosion, Wilson ***et al.*** (2007) and Fox ***et al.*** (2007a) measured ***in situ*** seepage flow and sediment concentrations along Little Topashaw Creek (LTC) and Goodwin Creek (GC), two deeply incised, fourth-order streams in northern Mississippi, followed by two-dimensional lysimeter (Figure 1-2) laboratory experiments used to mimic LTC and GC field conditions (soil layers packed proportionally). They found that sediment concentrations due to seepage erosion were correlated to the flow rate by a power law relationship and were directly proportional to the slope of the soil layers. The laboratory

experiments indicated that seepage begins minutes after flow initiation out of the bank face, resulting in substantial undercutting.

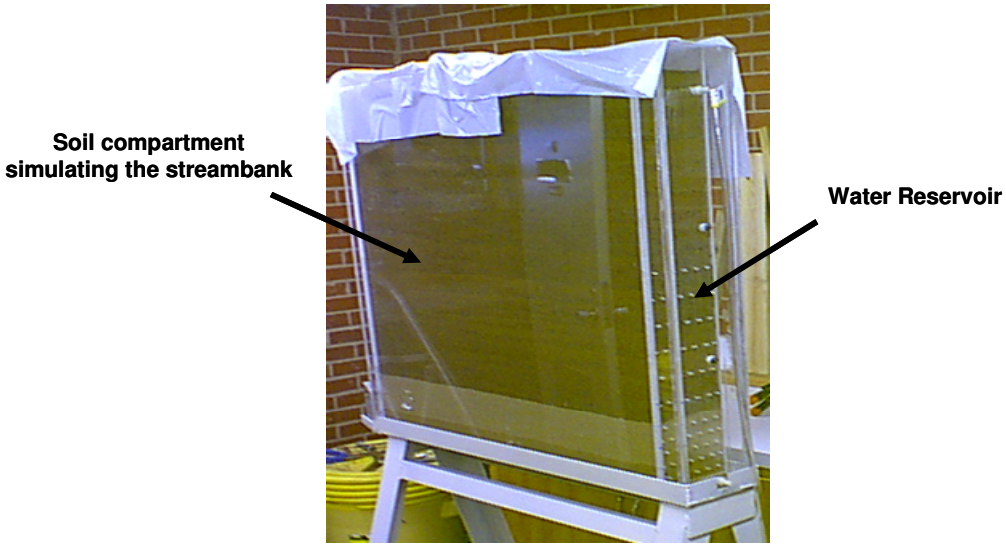

Figure 1-2. Two-dimensional lysimeter experiment to mimic *in situ* seepage erosion process (Fox *et al.*, 2006).

1.2 Vegetation

The impact of riparian vegetation on streambank stability has kept the interest of researchers for many years. It is well known that the stabilizing effects of vegetation include increased soil effective cohesion due to roots (by means of mechanical reinforcement and soil-moisture consumption) and precipitation interception via the canopy. Plants can also create destabilizing effects, such as increased near-surface moisture content due to greater infiltration from macropore formation along roots and higher surcharge due to the weight of the plant on the streambank (Simon and Collison, 2002).

In most cases, however, the stabilizing effects of vegetation are greater and more important to streambank stability and in the prevention of erosion than the destabilizing effects. Beeson and Doyle (1995) found that stream bends without vegetation were five times more likely as vegetated bends to have detectable erosion after flood events. Burckhardt and Todd (1998) further found that unforested concave banks have an average local migration rate three times greater than those concave banks that were forested. In general, channels with vegetated streambanks are narrow and stable and those with unvegetated banks are wide and unstable (Rowntree and Dollar, 1999; Huang and Nanson, 1997; Hey and Thorne, 1986).

The location and types of riparian vegetation on a streambank do not exhibit equal stabilizing effects. Huang and Nanson (1997) found that although dense vegetation on top of streambanks induced narrower channels, vegetation on the streambed increased flow resistance and reduced stream flow velocity, causing channel widening. Also, woody vegetation elements have a maximum impact on bank stability when they are located at the ends of the failure plane and when growing on low, shallow banks comprised of weakly cohesive sediments (van De Weil and Darby, 2007). Additionally, Trimble (1997) found that forested streambanks promote erosion more than grassed streambanks and these grassed channel reaches store 2100 to 8800 m^3 more sediment per km than forested reaches.

Grassed streambanks experience less erosion than forested streambanks due to a non-linear inverse relationship between root diameter and strength. This results in smaller roots contributing more strength per unit root area (Simon and Collison, 2002). Root fibers increase the shear strength of soils by transferring shear stresses that develop in the soil matrix into tensile resistance in the fiber inclusion via interface friction along the

length of the imbedded fibers (Gray and Sotir, 1996). Barker (1986) found that a root area ratio of 1 to 2% resulted in a 250% increase in shear strength of fiber-reinforced soil over non-reinforced soil. Deep, vertical taproots and sinker roots are the main contribution to stability when concerned about shallow sliding; therefore, grasses and shrubs have been found to be the optimum vegetation for riverbank and levee stabilization (Gray and Sotir, 1996; Simon and Collison, 2002).

1.3 Objective

Though ample consideration has been given to the effects of vegetation on streambank stability, very little is known about its effects on seepage erosion. The objective of this study is to analyze the effects of vegetation and root reinforcement on seepage erosion and undercutting, in regard to streambank stability, through the use of pre-existing modeling software and three-dimensional laboratory experiments. The results of these findings will ultimately help in the formation of a fully-incorporated dynamic streambank stability model.

1.4 Organization of Thesis

The organization of the chapters follows the chronological order of the development of ideas discussed in this thesis. It is necessary to note that some of the results contained in this thesis were published or submitted to international journals or conferences.

As summarized in the objective statement, two main ideas were investigated in the following chapters:

- Chapter 2 includes the numerical modeling of root reinforced streambanks in Version 4.1 of the USDA-ARS National Sedimentation Laboratory's Bank Stability and Toe Erosion Model (BSTEM). All vegetation available in the software was modeled on two streambanks that were extensively used in seepage erosion studies by previous authors. All contents of this chapter were included in a manuscript recently accepted for publication in *Earth Surface Processes and Landforms*: Cancienne R, Fox GA, Wilson GV. 2008. Influence of seepage undercutting on the stability of root reinforced streambanks. *Earth Surface Processes and Landforms* DOI: 10.1002/esp.1657.
- Chapter 3 includes the laboratory experiments conducted on a three-dimensional soil block, in which the shapes of seepage erosion undercutting were analyzed under different hydrologic conditions. Information about the laboratory set up and results are presented.
- Chapter 4 includes the laboratory experiments conducted on vegetated three-dimensional soil blocks. Switchgrass (*Panicum virgatum*) was planted and grown in soil blocks and the effects of root reinforcement on seepage erosion characteristics were analyzed. The information in this chapter will be presented at the American Society of Agricultural and Biological Engineers' (ASABE) Annual International Meeting in Providence, Rhode Island on June 29 to July 2, 2008.
- Chapter 5 gives general conclusions and future work is recommended.

CHAPTER II

INFLUENCE OF SEEPAGE UNDERCUTTING ON THE STABILITY OF ROOT REINFORCED STREAMBANKS

2.1 Abstract

Several mechanisms contribute to streambank failure including fluvial toe undercutting, reduced soil shear strength by increased soil pore-water pressure, and seepage erosion. Recent research has suggested that seepage erosion of noncohesive soil layers undercutting the banks may play an equivalent role in streambank failure to increased soil pore-water pressure. However, past research has primarily been limited to laboratory studies of nonvegetated banks. The objective of this research was to utilize the Bank Stability and Toe Erosion Model (BSTEM) to determine the importance of seepage undercutting relative to bank shear strength, bank angle, soil pore-water pressure, and root reinforcement. BSTEM was used to simulate two streambanks: Little Topashaw Creek (LTC) and Goodwin Creek (GC) in northern Mississippi. Simulations included three bank angles (70^{o} to 90^{o}), four pore-water pressure distributions (unsaturated, two partially saturated cases, and fully saturated), six distances of undercutting (0 to 40 cm), and thirteen different vegetation conditions (root cohesions from 0.0 to 15.0 kPa).

A relative sensitivity analysis suggested that BSTEM was approximately three to four times more sensitive to water table position than root cohesion or depth of seepage

undercutting. Seepage undercutting becomes a prominent bank failure mechanism on unsaturated to partially saturated streambanks with root reinforcement, even with undercutting distances as small as 20 cm. Consideration of seepage undercutting is less important under conditions of partially to fully saturated soil pore-water conditions. The distance at which instability by undercutting became equivalent to instability by increased soil-pore water pressure decreased as root reinforcement increased, with values typically ranging between 20 and 40 cm at LTC and between 20 and 55 cm at GC. This research depicts the baseline conditions at which seepage undercutting of vegetated streambanks needs to be considered for bank stability analyses.

2.2 Introduction

Sediment is a primary cause of water quality degradation with the majority of this sediment originating from streambanks in many watersheds. Research has demonstrated that streambank erosion and failure contributes significantly (i.e., up to 80%) to total sediment loading in streams (Bull and Kirkby, 1997; Simon and Darby, 1999; Sekely *et al*., 2002; Evans *et al*., 2006). Controlling sediment loading to surface water is important for the protection of human health and freshwater ecosystems; therefore, this sediment loading must be addressed through riparian management strategies.

Several mechanisms can lead to streambank failure and sediment loading to streams including toe erosion by streamflow undercutting the bank and bank sloughing by removal of matric suction (i.e., generation of positive pore-water pressure) due to precipitation infiltration or stream bank storage. When streambanks are saturated, stability is reduced (Darby *et al.*, 2007; Simon *et al.*, 2000; Rinaldi and Casagli, 1999;

Darby and Thorne, 1996). According to Hey *et al*. (1991), bank failures are characterized by either the shape or mode of failure. The Bank Stability and Toe Erosion Model (BSTEM), developed at the USDA-ARS National Sedimentation Laboratory (Simon and Collison, 2002), can simulate both planar and cantilever failures.

2.2.1 Seepage Erosion Undercutting

One of the processes that initiates mass failure and has received less attention is seepage erosion of noncohesive sediment by ground water flow, whereby lateral ground water emerges from the bank and undercuts the bank by removing soil particles (Fox *et al*., 2006; Fox *et al*., 2007a, 2007b; Wilson *et al*., 2007). Several studies report ground water sapping, where sapping is defined as the bank collapse resulting from seepage or piping erosion (Laity, 1983; Hagerty, 1991a, 1991b; Worman, 1993; Fox *et al*., 2007a, 2007b; Wilson *et al*., 2007). Seepage erosion occurs when high infiltration rates cause perched water tables to develop above water-restricting horizons in riparian soils (Coates, 1990; Wilson *et al*., 1991; Jones, 1997) or between layers with contrasting hydraulic conductivities (Hagerty, 1991a, 1991b). As perched water tables rise on these less permeable layers, sufficient hydraulic gradients can be generated towards stream channels, causing fairly rapid subsurface flow (interflow) towards streams. This lateral, subsurface flow can result in erosion of unconsolidated material at the outflow face (Higgins, 1982; Higgins, 1984; McLane, 1984; Dunne, 1990). Seepage flow initiates development and migration of headcuts by liquefaction of soil particles, followed by mass wasting of the stream bank by undercutting, as shown in Figure 2-1 (Fox *et al*.,

2006; Fox *et al*., 2007a, 2007b; Wilson *et al*., 2007). Hagerty (1991a, 1991b) suggest the formation of cavities accelerates the water supply to the exfiltration zone.

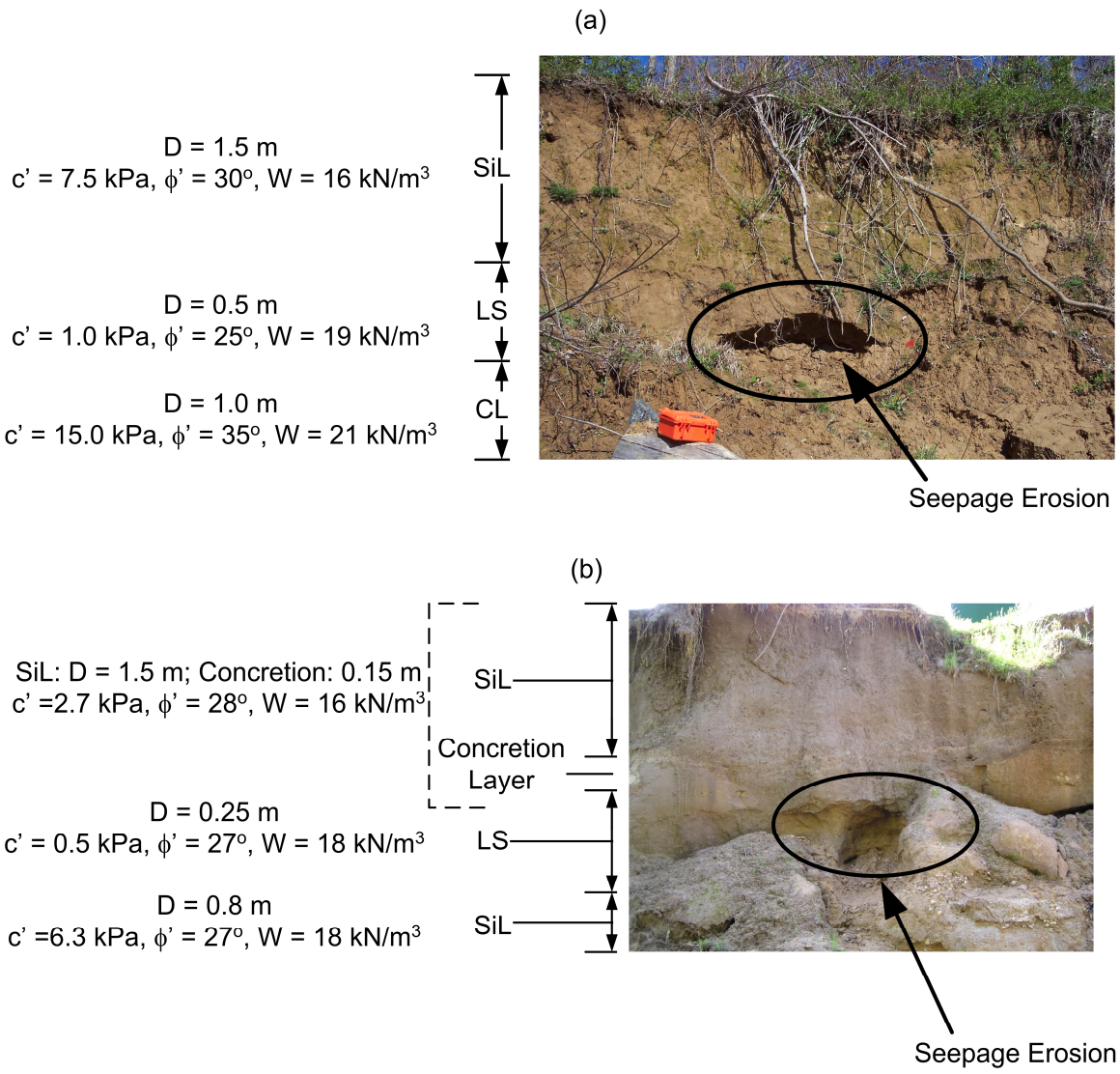

Figure 2-1. Stratigraphy of the (a) Little Topashaw Creek and (b) Goodwin Creek streambanks simulated using USDA-ARS bank stability model. Soil hydraulic and strength parameters are from Langendoen *et al*. (2005), Fox *et al*. (2007), and Chu-Agor *et al*. (2007). *D* is the depth of streambank layer; *c'* is the effective cohesion; *ϕ'* is the effective angle of internal friction; *W* is the unit weight; SiL is silt loam; LS is loamy sand; CL is clay loam.

Seepage erosion occurs in numerous geographical locations and has been shown to be an important mechanism of streambank failure (Chu-Agor *et al*., 2007). However, despite this frequent occurrence, little research has been performed regarding the effect of seepage undercutting on bank stability. Additionally, there is little understanding about the importance of seepage undercutting relative to other bank failure mechanisms. Wilson *et al*. (2007) simulated two-dimensional, laboratory lysimeter experiments using BSTEM by incorporating observed distances of undercutting. Their research indicated that the propensity of streambanks to fail during the recession limb of hydrographs may be the result of interflow-induced seepage erosion undercutting the streambanks, in addition to reduction in the soil shear strength. Chu-Agor *et al*. (2007) and Fox *et al*. (2007b) manually incorporated seepage undercutting into SLOPE/W to account for the interaction between reduced stability by increased pore-water pressure and seepage undercutting. Their work highlighted that the loss of supporting material brought about by seepage undercutting or hydraulic erosion at the bank toe can be a major cause of slope instability and may be of equal or greater importance than the impact of increased soil-water pressure on soil strength. It also highlighted the need to incorporate the dynamic process of seepage erosion into integrated subsurface flow and streambank stability models, but was limited to laboratory conditions, not predictions in the field. Darby *et al.* (2007) have coupled dynamic simulations of bank pore-water pressure with streambank stability models, but not specifically for seepage erosion undercutting.

2.2.2 Root Reinforcement

Research has also demonstrated that vegetation plays a role in bank stability, both advantageous and disadvantageous through root reinforcement, surcharge, and hydrologic influences, such as soil water uptake (Wu *et al*., 1979; Wu, 1984; Thorne, 1990; Beeson and Doyle, 1995; Gray and Sotir, 1996; Simon and Collison, 2002; Micheli and Kirchner, 2002; Pollen *et al*., 2004; Simon *et al*., 2006; Zaimes *et al*., 2006; Pollen, 2007). Both field and numerical modeling research has demonstrated that the addition of roots to streambanks improves stability under a range of hydrological conditions (Abernethy and Rutherfurd, 2000; Wynn *et al*., 2004; Simon *et al*., 2006; Pollen, 2007). Small amounts of root reinforcement can provide substantial increases in soil shear strength (Waldron, 1977; Wu *et al.*, 1988a, 1988b; Riestenberg, 1994). Pollen (2007) also noted that root reinforcement increased bank stability over a wide range of soil moisture conditions, but the magnitude varied as a function of soil shear strength and soil moisture content. Wynn and Mostaghimi (2006) discussed the influence of riparian vegetation on subaerial processes of freeze-thaw cycling and soil desiccation.

2.2.3 Objectives

Even with these recent advancements, we still do not understand the *in situ* conditions (i.e., variable soil moisture and vegetation regimes) at which seepage erosion and undercutting needs to be considered in bank stability analyses. In one of the only field studies of undercutting, Simon and Wells (2006) documented through repetitive surveys the amount and timing of erosion of a gulley headcut. They demonstrated that mass failure of the gulley headwall cannot occur unless the toe of the headcut had been

previously undercut by hydraulic erosion or cantilever failures. Fox *et al.* (2007a) observed that seepage undercutting distances of only 10 to 30 cm can result in bank collapse at Goodwin Creek. The objective of this research is to utilize BSTEM to quantify the interrelationship of pore-water pressure, vegetation, and seepage undercutting on bank stability. None of the recent research on bank instability by seepage erosion (i.e., Fox *et al.*, 2006; Fox *et al.*, 2007a, 2007b; Wilson *et al.*, 2007) has investigated root-reinforced streambanks. More specifically, this research addresses two questions: (1) what is the relationship between the factor of safety, *FS*, water table position (i.e., soil pore-water pressure distribution), and the distance of seepage undercutting as a function of root cohesion? and (2) Does the relative importance of undercutting versus increased soil-water pressure depend on root cohesion? Answering these questions will provide guidance as to when the inclusion of seepage undercutting of noncohesive streambank layers is required in bank stability analyses for river rehabilitation.

2.3 Materials and Methods

2.3.1 Streambank Stability Model

The main purpose of BSTEM is to predict whether or not a streambank will fail by accounting for fluvial undercutting, bank height, bank slope, the unit weight of soil and water in the bank, and surcharge created by objects on top of the bank. The greater resistance a bank has to failure by these forces, the greater its *FS*. BSTEM predicts this value by a variety of methods.

As the foundation of BSTEM, Simon *et al*. (2000) utilized the Mohr-Coulomb equation for the shear strength of saturated soil as follows:

$$\tau_f = c' + (\sigma - \mu_w)\tan\phi' \tag{2-1}$$

where τ_f is the shear stress at failure (kPa), c' is the effective cohesion (kPa), σ is the normal stress (kPa), μ_w is the pore-water pressure (kPa), and ϕ' is the effective angle of internal friction (degrees). In addition, since matric suction (negative pore-water pressure) above the water table increases soil cohesion, BSTEM defines the shear stress using the following equation from Fredlund and Rahardjo (1993):

$$\tau_f = c' + (\sigma - \mu_w)\tan\phi' + (\mu_a - \mu_w)\tan\phi^b \tag{2-2}$$

where μ_a is the pore-air pressure (kPa) and ϕ^b is the rate of increasing soil strength due to increasing matric suction (degrees). The parameter ϕ^b varies between soil types, typically ranging from 10^o to 20^o, reaching a maximum at ϕ' for saturation (Fredlund and Rahardjo, 1993).

Across horizontal layers, the model uses a limit equilibrium analysis that accounts for up to five user-input soil layers with unique geotechnical properties to calculate the *FS* as follows:

$$FS = \frac{\sum_{i=1}^{I}\left(c_i' L_i + S_i \tan\phi_i^b + \left[W_i\cos\beta - U_i + P_i\cos(\alpha-\beta)\right]\tan\phi_i'\right)}{\sum_{i=1}^{I}\left(W_i\sin\beta - P_i\sin[\alpha-\beta]\right)} \tag{2-3}$$

where c_i' is the effective cohesion of i^{th} layer (kPa), L_i is the length of the failure plane of the i^{th} layer (m), S_i is the force produced by matric suction on the unsaturated part of the failure surface (kN/m), W_i is the weight of the i^{th} layer (kN), U_i is the hydrostatic-uplift force on the saturated portion of the failure surface (kN/m), P_i is the hydrostatic-confining

force due to external water level (kN/m), β is the failure-plane angle (degrees from horizontal), α is the bank angle (degrees from horizontal), and I is the number of layers.

Along vertical slices, the model examines the normal and shear forces active in slices of the failure blocks (portions of the bank above the failure surface). This model incorporates a four-step iterative process that includes the normal force acting at the base of a slice, N_j, interslice normal force, I_{nj}, and interslice shear force, I_{sj}, to calculate FS using the following equation:

$$FS = \frac{\cos\beta \sum_{j=1}^{J} \left(c'_j L_j + S_j \tan\phi_j^b + \left[N_j - U_j \right] \tan\phi_j^{'} \right)}{\sin\beta \sum_{j=1}^{J} \left(N_j \right) - P_j} \tag{2-4}$$

where J is the total number of vertical slices. For cantilever shear failures, FS is merely a ratio of the shear strength of the soil layer(s) to the weight of the cantilever (overhanging soil layer or block):

$$FS = \frac{\sum_{i=1}^{I} \left(c'_i L_i + S_i \tan\phi_i^b - U_i \tan\phi_i^{'} \right)}{\sum_{i=1}^{I} \left(W_i - P_i \right)} \tag{2-5}$$

Since fibrous roots of vegetation are strong in tension, but weak in compression, their combined effects with soil (which is strong in compression, but weak in tension) create a fairly strong composite material (Wu *et al*., 1979; Wu, 1984; Thorne, 1990; Gray and Sotir, 1996; Micheli and Kirchner, 2002; Simon and Collison, 2002; Pollen *et al*., 2004; Simon *et al*., 2006; Pollen, 2007). Version 4.1 of the model uses the following fiber-break mode, force-equilibrium equation to calculate the increase in soil strength due to root systems:

$$c_r = T_r\left(A_r / A\right)\left(\cos\theta\tan\phi' + \sin\theta\right) \cong 1.2T_r\left(A_r / A\right) \quad (2\text{-}6)$$

where c_r is the cohesion due to roots (kPa), T_r is the tensile strength of roots (kPa), A_r/A is the area of shear surface occupied by roots, per unit area (root-area ratio), θ is the shear distortion from vertical (degrees), and ϕ' is the friction angle of soil (Waldron, 1977; Wu *et al.*, 1979; Waldron and Dakessian, 1981). This equation assumes perpendicular orientation of the roots relative to the shear failure plane. Gray and Sotir (1996) and Maher and Gray (1990) note that this assumption is useful because it represents an average of all possible root orientations. The assumption used in BSTEM is that roots of most riparian species are concentrated in the top 1 m of the soil profile (Simon *et al.*, 2007). Therefore, the effects of c_r on stability are equivalent to adding additional *c'* to the top 1 m of the bank. Pollen and Simon (2005) demonstrated that the above equations overestimate root reinforcement by up to 50% due to neglecting the fact that as the soil-root matrix shears, the roots have different tensile strengths and break progressively. Because of this anticipated 50% overestimation, Version 4.1 of BSTEM includes a vegetation safety margin which allows the user to adjust the maximum root reinforcement predicted by equation (2-6) by this factor.

Vegetation also decreases bank stability because of the negative effects of surcharge and increased infiltration into the soil profile. Surcharge increases normal stress due to an increase in mass acting on the surface. It can be calculated by multiplying the mass of the trees by the stocking density on the top of the bank from the DeVries (1974) equation. Default values of c_r and surcharge are provided in the USDA-ARS BSTEM for twelve vegetation species as outlined in Table 2-1. For this research, the

vegetation types were divided into three groups based on the estimated c_r after a 50% vegetation safety margin: 0-2.5 kPa, 2.5-5.0 kPa, and greater than 5.0 kPa.

Table 2-1. Types of vegetation and corresponding values of cohesion due to roots, c_r, and surcharge simulated on the Little Topashaw Creek (LTC) and Goodwin Creek (GC) streambanks with the USDA-ARS Bank Stability Model.

Cohesion Group	Vegetation Type	Cohesion (kPa)	Surcharge (kN/m^3)
0-5 kPa	Black Willow, *Salix nigra* (5 yrs)	2.0	0.6
	Sandbar Willow, *Salix exigua* (4 yrs)	3.0	0.6
	Sweetgum, *Liquidamber styraciflua* (10 yrs)	4.0	1.2
5-10 kPa	Himalayan Blackberry, *Rubus discolor* (5 yrs)	5.5	0.0
	Douglas Spirea, *Spirea douglasii* (3 yrs)	6.0	0.0
	Gamma Grass, *Tripsacum dactyloides* (5 yrs)	6.0	0.0
	Longleaf Pine, *Pinus palustris miller* (5 yrs)	6.0	0.6
	Sycamore, *Plantanus occidentalis* (7 yrs)	7.0	0.6
	Eastern Cottonwood, *Populus deltoides* (4 yrs)	8.0	0.6
	River Birch, *Betula nigra* (7 yrs)	8.0	0.6
>10 kPa	Alamo Switch Grass, *Panicum virgatum* L. (5 yrs)	18.0	0.0
	Western Cottonwood, *Populus fremontii* (14 yrs)	30.0	1.2

As an additional note on BSTEM, the *FS* is sensitive to shear surface angles. According to model documentation (Version 4.1), users have two options: (1) vary the shear angle to minimize the *FS* or (2) use the angle that is the average of the bank angle and the soil friction angle ϕ'. This research minimized the *FS* by varying the shear angle for each set of experimental conditions and compared the resulting angles to the latter

option above. Also, it should be noted that the model does not account for dynamic pore water pressures variations, shown to be important in triggering mass failures (Darby *et al.*, 2007).

2.3.2 Modeling of Field Sites

We simulated two streambanks with BSTEM: Little Topashaw Creek (LTC) and Goodwin Creek (GC) in northern Mississippi. LTC is an incised fourth-order stream near Calhoun City in central Mississippi (Stofleth *et al.*, 2007). Wilson *et al.* (2007) documented the first *in situ* detailed measurements of seepage flow, erosion, and bank undercutting along LTC. Fox *et al.* (2007a) conducted a similar study at GC, another incised stream which drains a fourth-order, 21 km^2 northwest Mississippi watershed near Batesville, Mississippi.

BSTEM was developed to simulate the top 300-cm bank of the streambank (i.e., above the noncohesive seepage layer) at LTC and the top 270-cm of the streambank (i.e., above the seepage layer) at GC with three different bank angles: 70^o, 80^o, and 90^o (Figure 2-1). A depiction of the stratigraphy, soil hydraulic parameters, soil strength parameters, and model setup for the LTC and GC banks is shown in Figure 2-1. Soil hydraulic and strength parameters for both sites were derived from Langendoen *et al.* (2005), Fox *et al.* (2007a), and Chu-Agor *et al.* (2007). Banks were simulated with no vegetation (c_r = 0 kPa and no surcharge) and then with default values for the twelve different vegetation species outlined in Table 2-1. A 50% vegetation safety margin, as suggested by Pollen and Simon (2005), was specified in the model to account for the overestimation of root reinforcement. Confining pressure due to stream stage was neglected; therefore, this

research simulated drawdown conditions at low-stream stages representative of conditions on the recession limb of streamflow hydrographs.

Model simulations included various distances (d_u) of hypothetical undercutting within the noncohesive streambank layers: no undercutting (d_u = 0 cm), d_u=5 cm, d_u=10 cm, d_u=20 cm, d_u=30 cm, and d_u=40 cm. The shapes of the undercuts used in the simulations were designed to give the smallest *FS* possible. Each undercut formed a triangle such that the elevation of the bottom of the triangle corresponded with the base of the simulated seepage layer (Figure 2-2). The heights of the triangles were consistent throughout simulations on each bank with the peak at the elevation of the top of the seepage layer. As the distance of undercutting increased with each simulation, the length of the base of the triangular cut increased to the corresponding distance. This mimics the undercut shapes utilized by Chu-Agor *et al*. (2007). The base of the failure surface was placed at the apex of the undercut as shown in Figure 2-2.

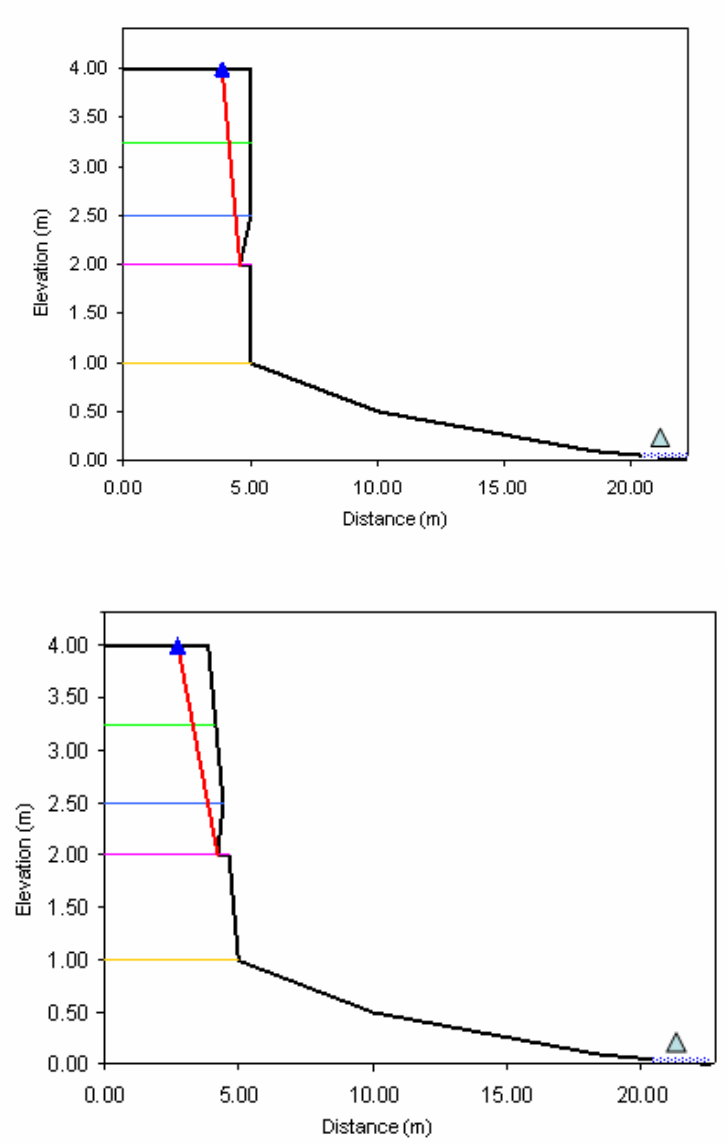

Figure 2-2. Example BSTEM simulation of LTC for (a) 90° and (b) 70° banks with d_u = 40 cm.

To investigate the influence of pore-water pressure on bank stability, we varied the position of the ground water table relative to the position of the seepage undercut layer. To simulate the influence of negative soil pore-water pressures on the soil shear strength, we used equation (2-2) with $\phi^b = 15^o$, the default value as suggested by BSTEM. Also, since the typical range reported for ϕ^b is generally between 10° and 20° (Fredlund and Rahardjo, 1993), we used $\phi^b = 15^o$ as the midpoint of the expected range. Four

different positions of the water table were simulated for each bank: unsaturated, two partially saturated cases, and a fully saturated case. For LTC, the 0.5-m, noncohesive seepage undercut layer occurred approximately 1.5 m below ground surface (bgs) (Wilson *et al*., 2007). Therefore, simulations were performed with the ground water table at 2.00 m bgs (unsaturated, 0% of the bank height, BH, where bank height refers to height above the bottom of the seepage layer), 1.50 m bgs (partially saturated, 25% of the BH), 1.00 m bgs (partially saturated, 50% of the BH), and saturated (100% of the BH). For GC, the 0.25-m, noncohesive seepage undercut layer occurred 1.65 m bgs (Fox *et al*., 2007a). Simulations included the ground water table at 1.90 m bgs (unsaturated, 0% of the BH), 1.43 m bgs (partially saturated, 27% of the BH), 0.95 m bgs (partially saturated, 50% of the BH), and saturated (100% of the BH). Tension cracks, while known to further reduce the stability of banks, were not included in these simulations. BSTEM can simulate tension cracks but requires the user to specify the tension crack depth, which for these hypothetical scenarios could only be estimated or assumed. Therefore, the total number of BSTEM simulations was 1,872: two banks, three bank angles, four water table positions, six distances of undercutting, and thirteen different vegetation conditions.

2.3.3 Analysis of Modeling Results

The relative sensitivity (S_r) of c_r, d_u, and water table position was calculated based on the following equation:

$$S_r = \left(\frac{\frac{\partial O}{O}}{\frac{\partial P}{P}} \right) = \left(\frac{O - O_b}{P - P_b} \right) \left(\frac{P_b}{O_b} \right) \tag{2-7}$$

where O is the output (i.e., the FS), P is in the input, and the subscript b represents the base value (Byne, 2000). The base line condition for the relative sensitivity analysis was a 70^{o} bank with c_r = 3.0 kPa, d_u = 10 cm, and WT = 1.50 m bgs for LTC and WT = 1.43 m bgs for GC. The c_r, d_u, and water table position were varied within the range of -67% to 200% of the original base value.

The next question to be addressed was the relation between the FS and the distance of undercutting for a given c_r value. For both banks, the predicted FS values were first plotted against the ratio of the distance of undercutting and bank height (d_u/BH) above the seepage layer for the various vegetation types with a 50% vegetation safety margin (Table 2-1). As a comparison, similar figures were developed for the relationship between the FS and the height of the water table relative to BH. A critical distance of undercutting (d_u*) required to reach conditionally unstable conditions (i.e., FS = 1.3) was determined based on the FS-d_u/BH plots for each root cohesion value. The d_u* was non-dimensionalized by the BH and then plotted against the ratio of c_r to the effective cohesion, c', of each bank. This analysis generated information regarding the d_u* relative to bank angle, soil pore-water pressure distribution, and root cohesion.

The final question involved the relative importance of undercutting and increased soil-water pressure, investigated in prior research by Fox *et al*. (2006), Fox *et al*. (2007b), and Wilson *et al*. (2007), in which they suggested that undercutting can possess equivalent or greater importance than increased soil pore-water pressure at some critical distance of undercutting. This research adds another complicating factor in terms of vegetation. The importance of undercutting and soil pore-water pressure at different c_r was determined by calculating the variation in the FS if one of these processes was

neglected. More specifically, for each case of bank slope, d_u, water table position, and c_r (e.g., slope = 90°, d_u = 20 cm, water table position = 50% of the BH, and c_r = 8.0 kPa), the predicted *FS* was assumed to be the "true" *FS*. Two alternative *FS* were determined for this scenario by (1) neglecting undercutting (e.g., d_u = 0 cm, water table position = 50% of the BH, and all other parameters held constant) and then by (2) neglecting potential rises in the water table position above the seepage layer (e.g., water table position = 0% of the BH, d_u = 20 cm, and all other parameters held constant). The error in the *FS* was calculated between the "true" *FS* and the two alternative *FS*. The alternative *FS* with the greater error corresponded to the most important process for these conditions (i.e., undercutting versus increased soil pore-water pressure). By considering all possible d_u, water table, and c_r combinations, it was determined whether root cohesion affected the point at which undercutting possessed equal importance to increased soil pore-water pressure. The d_u for which the error in neglecting undercutting became greater than the error in neglecting soil pore-water pressure effects, referred to hereafter as d_{us}, was determined.

2.4 Results and Discussion

The predicted *FS* decreased as α, μ_w, and d_u increased and as the c_r decreased (Table 2-2). The reported increase in the *FS* relative to addition of roots is equivalent to that reported in other research with BSTEM and other slope stability models (e.g., Abernethy and Rutherfurd, 2000; Simon *et al*., 2006; Pollen, 2007). Cohesion due to roots was a more important parameter than surcharge for simulating reinforcement under the conditions modeled. Minimal differences were observed in the predicted *FS* for

vegetation types with the same cohesion but different surcharge (i.e., Douglas spirea, Gamma grass, and longleaf pine). For the LTC and GC banks, the maximum difference in the predicted *FS* between the three species listed above was consistently less than 0.10, with these differences decreasing as undercutting increased.

Failure plane angles resulting in the minimum *FS* were greater at GC as compared to LTC under similar water table, undercutting, and bank slope conditions because of the lower c' and ϕ' at GC. The shear angles increased as d_u and α increased and decreased as c_r increased (Table 2-3). The data suggests that shear angle is much more sensitive to d_u as compared to c_r and water table position, as the shear angles were independent of water table position. The shear angles resulting in the minimum *FS* typically bounded the theoretical angle suggested by the average of α and ϕ'.

The S_r analysis for both LTC and GC banks suggested that the model was most sensitivity to water table position (i.e., S_r = 0.4 to 0.6). BSTEM was approximately three to four times more sensitive to water table position than c_r and d_u (Table 2-4). These results emphasize the importance of appropriately simulating the pore-water pressure distribution for stability analyses as suggested by previous researchers (Darby *et al.*, 2007; Simon *et al.*, 2000; Rinaldi and Casagli, 1999; Darby and Thorne, 1996). The S_r of the model was approximately equivalent (i.e., S_r = 0.1 to 0.2) for c_r and d_u at both streambanks (Table 2-4). Results were similar for other bank angles.

Table 2-2. Predicted *FS* for LTC and GC streambanks at various bank angles (α) and depth of undercutting (d_u) as a function of root cohesion (c_r) and water table position. The two *FS* values under each c_r value are for unsaturated conditions (i.e. water table at the bottom of the seepage layer) and partially saturated conditions (i.e., water table at 50% of the bank height above the seepage layer), respectively.

Stream	α	d_u	c_r (kPa)			
	(^{o})	(cm)	0	0-5	5-10	>10
LTC	90	0	1.6, 1.1	1.6, 1.2	1.8, 1.3	2.3, 1.9
		10	1.4, 1.0	1.5, 1.1	1.6, 1.2	2.1, 1.7
		20	1.3, 0.9	1.4, 1.0	1.5, 1.1	1.9, 1.6
		40	1.1, 0.7	1.1, 0.8	1.2, 0.9	1.6, 1.3
	80	0	1.9, 1.4	2.0, 1.4	2.1, 1.6	2.8, 2.2
		10	1.7, 1.2	1.8, 1.3	1.9, 1.5	2.5, 2.0
		20	1.6, 1.1	1.6, 1.2	1.8, 1.3	2.3, 1.9
		40	1.3, 0.9	1.3, 1.0	1.5, 1.1	1.9, 1.5
	70	0	2.3, 1.6	2.4, 1.8	2.6, 2.0	3.4, 2.7
		10	2.1, 1.5	2.2, 1.6	2.4, 1.8	3.1, 2.5
		20	1.9, 1.4	2.0, 1.5	2.2, 1.6	2.8, 2.3
		40	1.6, 1.1	1.7, 1.2	1.8, 1.3	2.4, 1.9
GC	90	0	1.1, 0.6	1.2, 0.7	1.3, 0.9	2.0, 1.5
		10	1.0, 0.5	1.1, 0.6	1.2, 0.8	1.8, 1.4
		20	0.9, 0.5	0.9, 0.6	1.1, 0.7	1.6, 1.2
		40	0.7, 0.4	0.8, 0.4	0.9, 0.6	1.3, 1.0
	80	0	1.3, 0.8	1.4, 0.9	1.6, 1.1	2.4, 1.8
		10	1.2, 0.7	1.3, 0.8	1.5, 1.0	2.1, 1.7
		20	1.1, 0.6	1.2, 0.7	1.3, 0.9	1.9, 1.5
		40	0.8, 0.5	0.9, 0.6	1.1, 0.7	1.6, 1.2
	70	0	1.6, 1.0	1.7, 1.1	1.9, 1.3	2.8, 2.2
		10	1.4, 0.9	1.6, 1.0	1.8, 1.2	2.6, 2.0
		20	1.3, 0.8	1.4, 0.9	1.6, 1.1	2.3, 1.8
		40	1.0, 0.6	1.1, 0.7	1.3, 0.9	1.9, 1.5

Table 2-3. Shear failure plane angle (degrees) resulting in the minimum factor of safety for LTC and GC streambanks as a function of bank angle (α), depth of undercutting (d_u), and root cohesion (c_r), and comparison to theoretical shear failure plane angle based on average of α and the internal friction angle (ϕ').

Stream	α	d_u	c_r (kPa)				Theoretical
	(^{o})	(cm)	0	0-5	5-10	>10	($\phi'+\alpha$)/2
LTC	90	0	55	55	55	50	60
		10	55	55	55	55	
		20	60	60	60	60	
		40	70	70	70	65	
	80	0	47	47	47	46	55
		10	50	50	50	50	
		20	55	55	55	52	
		40	60	60	60	60	
	70	0	43	42	40	40	50
		10	45	45	45	43	
		20	48	48	48	47	
		40	53	53	53	52	
GC	90	0	60	59	57	53	59
		10	65	63	60	56	
		20	68	65	65	61	
		40	77	75	73	68	
	80	0	52	50	50	47	54
		10	55	55	55	50	
		20	60	59	58	54	
		40	68	67	65	61	
	70	0	45	45	43	41	49
		10	48	48	47	43	
		20	52	52	50	47	
		40	60	60	57	54	

Table 2-4. Relative sensitivity of BSTEM relative to root cohesion (c_r), depth of undercutting (d_u) and water table position (WT, m below ground surface, bgs) for Little Topashaw Creek (LTC) and Goodwin Creek (GC) streambanks. The baseline condition for the relative sensitivity analysis was a 70° bank with c_r = 3.0 kPa, d_u = 10 cm, and WT = 1.50 m bgs for LTC and WT = 1.43 m bgs for GC.

Streambank Site	Parameter		Parameter Value	Factor of Safety (*FS*)	Relative Sensitivity
LTC	c_r	Baseline	3.0	2.08	
	(kPa)	-67%	1.0	1.87	0.2
		-50%	1.5	1.91	0.2
		+33%	4.0	2.13	0.1
		+200%	9.0	2.61	0.1
	d_u	Baseline	10	2.08	
	(cm)	-50%	5	2.18	-0.1
		+100%	20	1.90	-0.1
		+200%	30	1.73	-0.1
	WT	Baseline	1.50	2.08	
	(m bgs)	-33%	1.00	1.76	0.5
		+33%	2.00	2.36	0.4
GC	c_r	Baseline	3.0	1.46	
	(kPa)	-67%	1.0	1.24	0.2
		-50%	1.5	1.29	0.2
		+33%	4.0	1.53	0.1
		+200%	9.0	2.05	0.2
	d_u	Baseline	10	1.46	
	(cm)	-50%	5	1.54	-0.1
		+100%	20	1.32	-0.1
		+200%	30	1.18	-0.1
	WT	Baseline	1.43	1.46	
	(m bgs)	-33%	0.95	1.17	0.6
		+33%	1.90	1.74	0.6

2.4.1 Influence of Undercutting and Pore-Water Pressure on Stability

The relation between the *FS* and the d_u/BH ratio was linear to slightly exponential (Figure 2-3); similar observations were made by Chu-Agor *et al*. (2007) in modeling

controlled laboratory experiments of bank instability by undercutting. For a 90° LTC bank (c' = 7.5 kPa in the top 1.5 m of the bank) with no vegetation and unsaturated flow conditions, the bank becomes conditionally unstable with 20 cm of undercutting and unstable (i.e., FS = 1.0) with approximately 46 cm of undercutting. The GC bank (c' = 2.7 kPa in the top 1.5 m of the bank) with a 90° bank angle was initially conditionally unstable unless the bank possessed vegetation with c_r greater than 2.5 kPa (Figure 2-3).

Even small degrees of undercutting can counteract the effects of root reinforcement by vegetation with assumed root depths of 1 m. For example, under unsaturated conditions, LTC or GC 90° vegetated banks with c_r of less than 2.5 kPa were equivalent to a bank without vegetation when the distance of undercutting was approximately 3 to 7 cm on the vegetated bank (Figure 2-3). For banks with c_r between 2.5 and 5.0 kPa, instability was equivalent to a bank without vegetation when the distance of undercutting was approximately 15 to 20 cm. Such degrees of undercutting are well within the range of maximum observed distances of seepage undercutting in the field (i.e., 10 to 30 cm) as reported by Fox *et al*. (2007a) at GC and Wilson *et al*. (2007) at LTC.

The FS decreased linearly with increases in the height of the water table relative to the bottom of the seepage layer (Figure 2-4). These results mimic those of Pollen (2007) in that the effects or impacts of a given magnitude of root reinforcement varied relative to soil shear strength and soil moisture. With a partially saturated bank (i.e., water table at 50% of the BH above the seepage layer), a LTC or GC bank without vegetation or with c_r less than 2.5 kPa was conditionally unstable without undercutting (Figure 2-4).

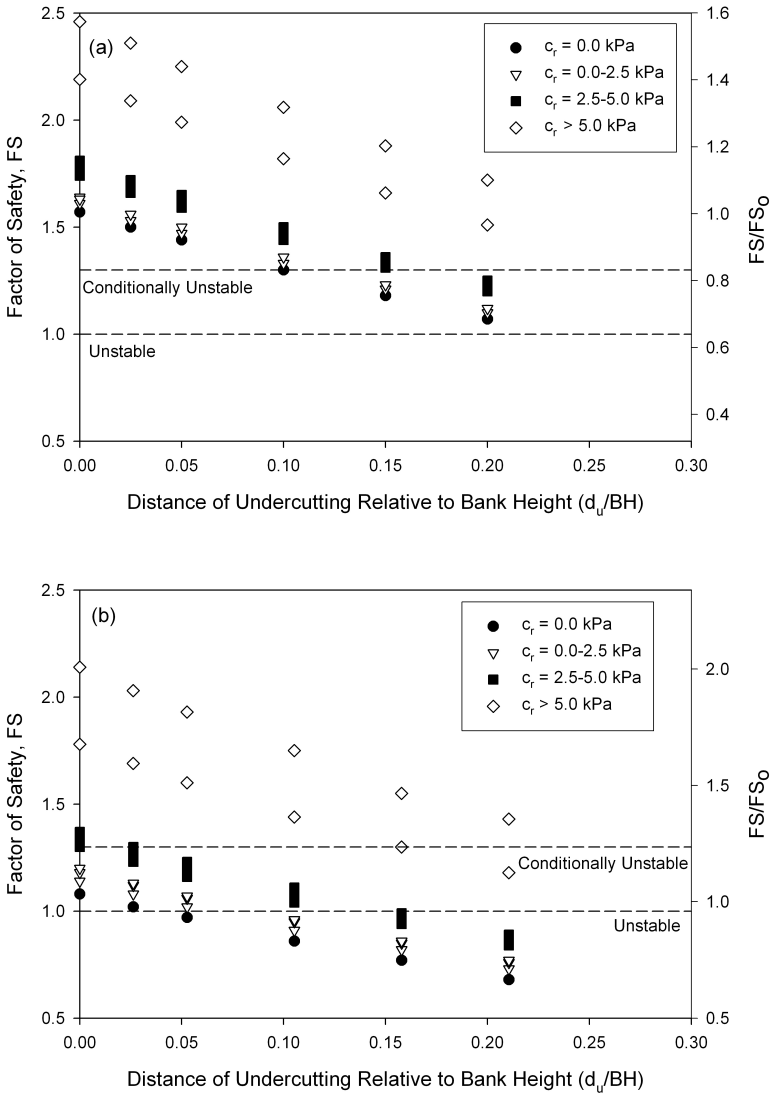

Figure 2-3. Predicted factor of safety, *FS*, versus the depth of undercutting (d_u) non-dimensionalized by the bank height above the seepage layer (BH) for various values of root cohesion, c_r, for 90^o (a) LTC and (b) GC banks and for unsaturated soil pore-water pressure conditions (i.e., water table at bottom of the seepage layer).

Such results suggest consideration of seepage undercutting is critical for bank stability analyses under unsaturated to partially saturated soil pore-water pressure distributions and is less important under conditions of partially to fully saturated soil pore-water conditions. Saturation conditions result in a reduction in the shear strength of the soil that supersedes the instability due to undercutting investigated in this research.

However, seepage flow and undercutting have been reported to occur in the field under unsaturated to partially saturated hydrologic regimes (Fox *et al*., 2007a). In one of the only reported field studies of streambank seepage in conjunction with riparian pore-water pressure measurements, Fox *et al*. (2007a) report over a month of data where seepage flow/undercutting occurred with negative pore-water pressures in the bank material above the seepage horizon.

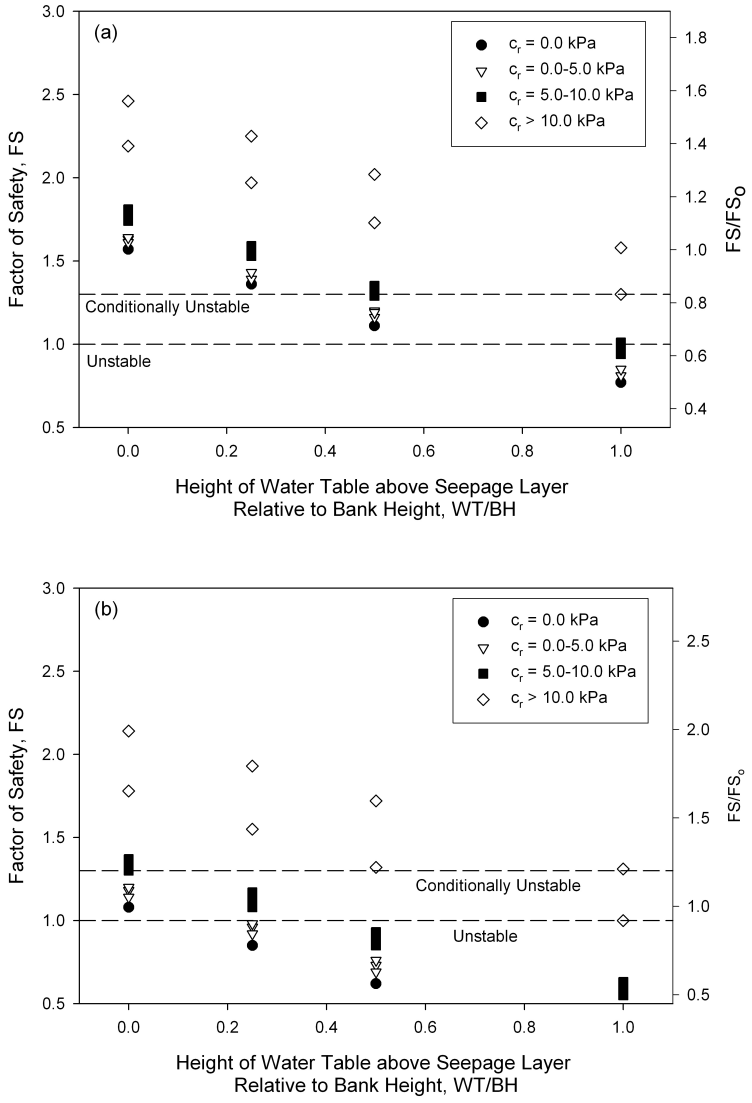

Figure 2-4. Predicted factor of safety, *FS*, versus the water table height (WT) non-dimensionalized by the bank height above the seepage layer (BH) for various values of root cohesion, c_r, for 90^o (a) LTC and (b) GC banks and for no undercutting.

2.4.2 Critical Distance of Undercutting for Conditionally Unstable Conditions

For both banks, the critical d_u required to reach conditionally unstable conditions (FS = 1.3) with unsaturated pore-water pressures increased logarithmically with c_r/c', approaching an asymptote with increases in c_r/c' (Figure 2-5). Greater c_r/c' represents a reinforced bank that requires larger undercutting distances to reduce the FS. The d_u required to reach conditionally unstable banks were approximately 20 cm at LTC and 0 cm (i.e., no undercutting) at GC for 90^o bank angles and approximately 38 cm at LTC and 2 cm at GC for 80^o bank angles without vegetation. For root cohesions of approximately 5.0 kPa, the critical distances of undercutting increased to approximately 35 cm at LTC and 5 cm at GC for 90^o angles and approximately 55 cm at LTC and 25 cm at GC for 80^o angles. Differences between BSTEM predictions for LTC and GC banks were due to the greater c' and ϕ', and correspondingly τ_f, at LTC as compared to GC.

Bank slope appeared to influence the critical distance of undercutting uniformly across the range of c_r investigated (Figure 2-5). More specifically, the increase in d_u*/BH was approximately 0.1 with 10^o decreases in the bank angle. As soil pore-water pressure increased (i.e., banks became saturated), the d_u*/BH decreased for all c_r/c' due to the additional reduced shear strength caused by the increase in μ_w. The influence of water table position on d_u*/BH was not uniform across c_r. The difference between pore-water pressure curves increased as c_r decreased (Figure 2-6), suggesting that the interrelationship between water table position and undercutting was more important at lower c_r because of the banks' lower reinforced strength.

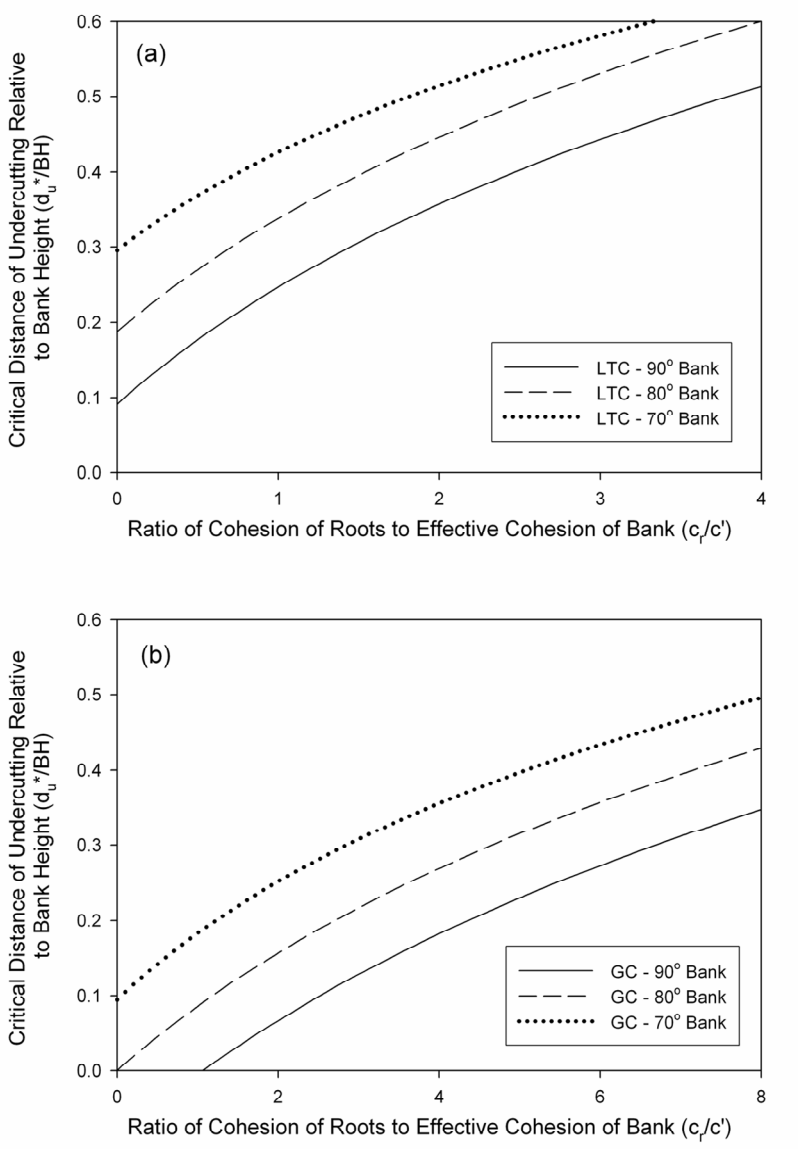

Figure 2-5. Ratio of critical undercut depth (i.e., depth of undercutting required to reach conditionally unstable conditions), d_u*, relative to cohesion by vegetation for varying bank slopes at (a) LTC and (b) GC assuming unsaturated conditions (i.e., water table at the bottom of the seepage layer).

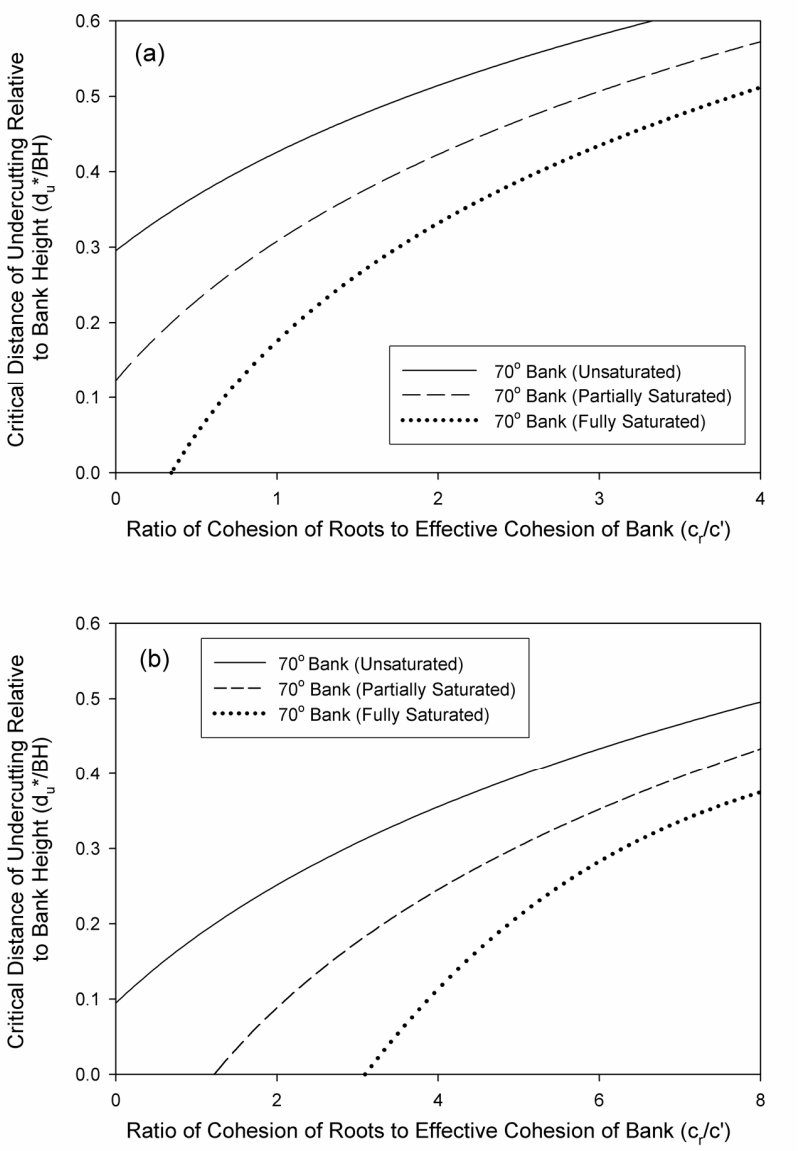

Figure 2-6. Ratio of critical undercut depth, d_u*, relative to cohesion by vegetation for varying soil pore-water pressure distributions at (a) LTC and (b) GC for a 70° bank angle. Unsaturated conditions refer to a bank with a water table at the bottom of the seepage layer.

2.4.3 Instability by Undercutting versus Soil Pore-Water Pressure

For a specific c_r/c' in Figure 2-7, the region above each line represents conditions where the undercut geometry (i.e., d_u) is more important than the pore water pressure (i.e., WT/BH) in determining the *FS* whereas the region below each line represents

conditions where pore water pressure is more important. The d_{us} appeared independent of bank slope for the conditions modeled (Figure 2-7a). The d_{us} was greater at GC than LTC because of the c' of the banks (Figure 2-7). Increases in soil pore-water pressure reduced the stability of the less cohesive GC bank (c' = 2.7 kPa) more so than the LTC bank (c' = 7.5 kPa).

Consistent among both banks is the fact that undercutting becomes a prominent bank failure mechanism on unsaturated to partially saturated streambanks with greater root reinforcement, even with undercutting distances as small as 20 cm. For LTC banks under partially saturated conditions (i.e., WT/BH = 50%), neglecting undercutting led to a greater error in the predicted *FS* when d_{us} was between 20 and 40 cm, with this distance decreasing as c_r increased (Figure 2-7a). These distances fall well within the range of observed undercutting distances at LTC (Wilson *et al.*, 2007). For GC banks under similar conditions, the corresponding d_{us} were less than 20 cm for c_r/c' greater than 5.0 to greater than 55 cm for c_r/c' less than 0.5 (Figure 2-7b). Under partially saturated conditions with WT/BH = 25%, d_{us} decreased to less than 20 cm for both streambanks. Alternatively, for saturated conditions (i.e., WT/BH = 100%), neglecting pore-water pressure effects resulted in greater errors in the predicted *FS* for all c_r unless d_{us} approached 100 cm (Figure 2-7b). Such undercutting distances have not been reported in any field monitoring studies.

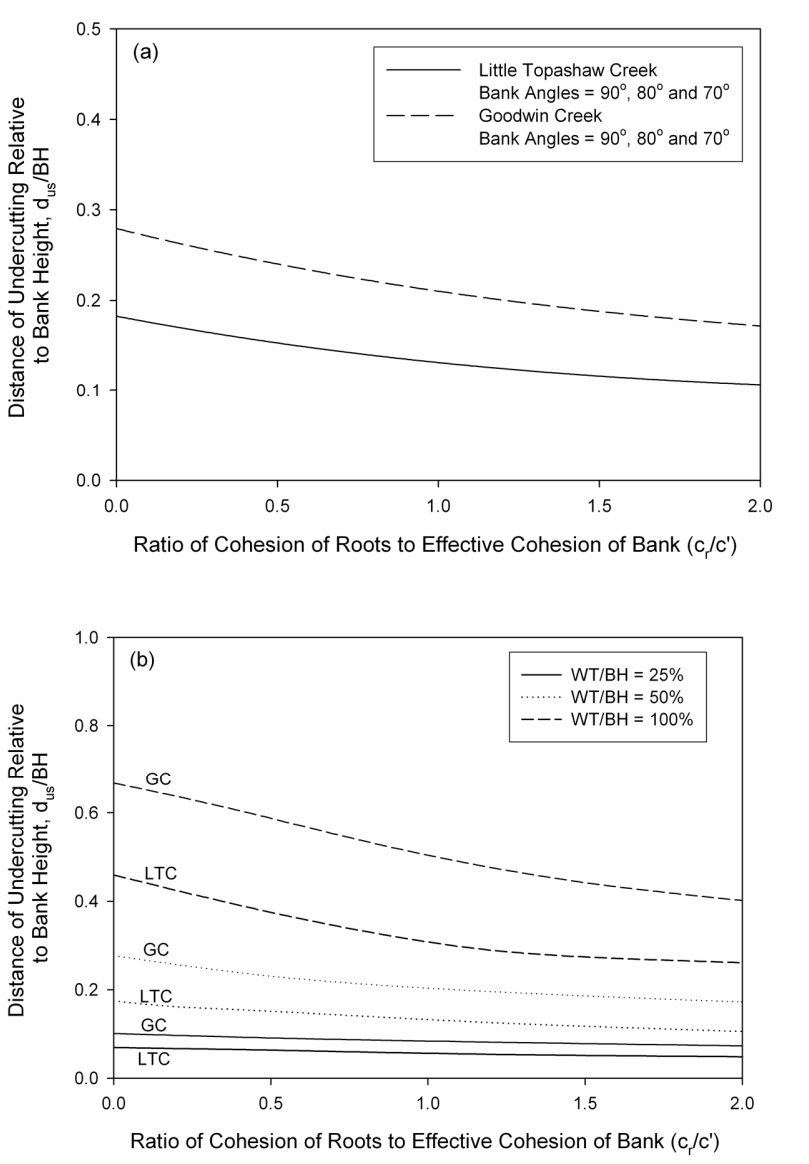

Figure 2-7. Depth of undercutting, d_{us}, at which the influence of undercutting on stability becomes greater than the influence of soil pore-water pressure relative to root cohesion for (a) various slopes (with water table at 50% of the bank height), and (b) various water table depths for a 80° bank at LTC and GC. BH is the bank height above the seepage layer. The region above each line represents conditions where the undercut geometry is more important than the pore water pressure; whereas, the region below each line represents conditions where pore water pressure is more important. The vegetation safety margin was applied to c_r.

2.5 Conclusions

As expected, the predicted *FS* decreased with increasing bank angle, soil pore-water pressure, and distance of undercutting and decreasing root reinforcement for both the LTC and GC simulated streambanks. The *FS* decreased linearly or slightly exponentially with increasing distances of undercutting. The *FS* also decreased linearly with increasing water table elevation relative to the elevation of the base of the seepage layer. BSTEM was most sensitive to water table position. In fact, the model was approximately three to four times more sensitive to water table position than root cohesion or depth of seepage undercutting, with BSTEM being equivalently sensitive to these last two parameters. Consideration of the effects of undercutting during unsaturated flow conditions becomes critical for bank stability analysis with very small undercut distances, even with additional cohesion in the top 1.0 m from vegetation; however, these effects become less important under partially to fully saturated soil pore-water conditions because the loss of strength from increased soil pore-water pressure offsets the increase in strength due to c_r. The undercutting distances at which the error in neglecting undercutting became greater than the error in neglecting soil pore-water pressure effects on soil shear strength generally ranged between 20 and 55 cm among the two simulated streambanks and was independent of bank slope. Undercutting tended to be the more prominent bank failure mechanism at smaller distances of undercutting with greater root reinforcement. Due to all of the possible variables involved in streambank stability analysis and cases of river rehabilitation in which young, immature vegetation may be used for root reinforcement, a need exists for streambank stability models that can

analyze for site-specific failure processes, including seepage undercutting of non-cohesive streambank layers.

CHAPTER III

LABORATORY EXPERIMENTS OF THREE-DIMENSIONAL SEEPAGE EROSION UNDERCUTTING

3.1 Abstract

Although seepage erosion has three-dimensional characteristics, two-dimensional lysimeters have been used in previous research to analyze for the hydraulic and geotechnical controls on this mechanism of hillslope, gully, and bank instability. A 50 cm cubic soil block with a focused inflow reservoir was constructed to investigate the mechanisms of seepage erosion and the three-dimensional nature of seepage undercutting. Experiments included 25-cm tall, sand and loamy sand banks cut at various angles (90^o, 75^o, and 60^o) and packed at prescribed bulk densities (1.30 to 1.70 g cm^{-3}). Constant heads of 15 cm, 25 cm, and 35 cm were imposed on the soil to induce flow. A laser scanner was utilized to obtain the three-dimensional coordinates of the bank and undercut surfaces at approximately 15 to 30 s intervals. For cases experiencing particle mobilization and undercutting, seepage erosion initiated as unimodal (i.e., concentrated at one point) or as multimodal (i.e., initiating at several locations across the bank face), and was largely controlled by the bank angle. As a first approximation, a three-dimensional, five-parameter Gaussian distribution was fit to the undercut shapes to derive parameters for the maximum depth of undercutting, position of the center of the peak, and the

vertical and lateral spreads of the undercut. Trends from this analysis will assist in the development of improved sediment transport functions and the incorporation of this failure mechanism into stability models.

3.2 Introduction

Seepage erosion has been suggested to potentially play a prominent role in gully and streambank erosion. Subsurface erosion, particularly piping, is now accepted as a critically important process in rill and gully development, especially in Europe (Faulkner, 2006; Sultan *et al.*, 2004). Although seepage erosion has been observed to occur before massive bank slumping (Bradford and Piest, 1977), it was not until recently that it has been highlighted as a potential failure mechanism of streambanks particularly on the recession limb of the streamflow hydrographs (Fox *et al*., 2007a; Wilson *et al*., 2007).

The complex interaction between seepage and other bank failure mechanisms makes it difficult to fully understand the role of seepage on bank instability. According to Crosta and di Prisco (1999), in order to understand the onset of streambank instability due to seepage, it is important to point out that the collapse is the final result of a complex chain of events taking place during a certain time period. They added that analysis is complex because of the partial saturation of the materials, the three-dimensional geometry of the problem, and the heterogeneity of materials. Hooke (1979) suggested that more detailed work is needed on the mechanics of the processes to identify the effects of soil moisture, the pattern of forces on the bank and the changes in shear strength of the bank material. The ASCE Task Committee on Hydraulics, Bank Mechanics, and Modeling of River Adjustments (1998) suggested that methods capable

of predicting the stability of streambanks with respect to a range of possible failure mechanisms must be developed.

Slope instability due to increase in pore-water pressure brought about by seepage has been well documented to cause bank instability (Abam, 1993; Darby and Thorne, 1996; Crosta and di Prisco, 1999; Rinaldi and Casagli, 1999; Simon *et al.*., 1999). Soil strength or the resisting force which is responsible for bank stability is usually defined using Mohr-Coulomb's equation:

$$\tau_f = c' + (\sigma - \mu_w)\tan\phi' \tag{3-1}$$

where τ_f is the shear stress at failure (kPa), c' is the effective cohesion (kPa), ϕ' is the effective angle of internal friction (degrees), σ is the total normal stress (kPa), and μ_w is the soil pore-water pressure (kPa) (Whitlow, 1983; Fredlund and Rahardjo, 1993). In unsaturated soils, increasing matric suction has the effect of increasing the apparent cohesion of the soil, as described by Fredlund and Rahardjo (1993):

$$\tau_f = c' + (\sigma - \mu_w)\tan\phi' + (\mu_a - \mu_w)\tan\phi^b \tag{3-2}$$

where μ_a is the soil pore-air pressure (kPa) and ϕ^b is the angle indicating the rate of increase in the shear strength relative to matric suction and is generally between 10^o and 20^o. Therefore, an increase in pore-water pressure decreases the effective stress of the soil which in turn decreases the shear strength. Seepage force, which is one of the driving or destabilizing forces, acts on grains of sediment and is proportional to the hydraulic gradient $\frac{\partial \psi}{\partial y}$ where ψ is the matric suction and y is a distance:

$$\tau_s = \rho g d \frac{\partial \psi}{\partial y} \tag{3-3}$$

where τ_s is the seepage stress (kPa), ρ is the density of the fluid (kg m^{-3}), g is gravity (m s^{-2}), and d is the grain diameter (m). Several studies have incorporated this seepage force into equations for particle mobilization by seepage such as Lobkovsky *et al*. (2004) who modified the Shields number to include this seepage force.

Despite the research conducted on bank instability by increased soil pore-water pressure and tension or "pop-out" failure by seepage forces, bank failure due to seepage particle mobilization (i.e., entrainment in the seepage flow) has not been fully investigated. On banks with enough resistance to overcome seepage forces, the seepage gradient can cause particle mobilization when the velocity of water exiting the bank exceeds the critical shear stress leading to bank undercutting. This failure mechanism was studied by Fox *et al*. (2006, 2007a, 2007b) and Wilson *et al*. (2007) in their two-dimensional lysimeter experiments and bank stability modeling. Fox *et al*. (2006) derived a sediment transport function using data from these two-dimensional lysimeter experiments.

In this study, the hydraulic conditions producing these seepage failure mechanisms were evaluated and the three-dimensional nature of seepage erosion was investigated. There has been work on the effect of changes in the geometry of a hillslope or bank due to undercutting on failure such as the static analyses reported by Wilson *et al*. (2007) and the step-wise dynamic analysis by Chu-Agor *et al*. (2007). A fully integrated variably saturated flow model with a dynamic geometric and geotechnical model to predict hillslope, gully or bank failure is still lacking. Knowledge on the three-dimensional structure of seepage entrainment and undercutting is needed for this dynamic hydraulic and geotechnical modeling.

3.3 Materials and Methods

3.3.1 Experimental Setup and Data Analysis

A three-dimensional soil block was constructed from clear acrylic glass with dimensions 50 cm by 50 cm by 50 cm (Figure 3-1). The block has two compartments: a focused water reservoir (10 cm high by 10 cm wide centered at the bottom of the back face of the soil block) where a constant water head is maintained and the soil compartment which simulates a single layered hillslope, gully sidewall, or streambank with varying bank angles (α). Two different types of soil were used for these experiments: sand and loamy sand. Each soil type was packed in the box at various bulk densities (ρ_b): 1.30, 1.45, and 1.60 g cm^{-3} for the sand and 1.30, 1.45, 1.50, 1.60, and 1.70 g cm^{-3} for the loamy sand. All experiments consisted of soil blocks with heights of 25 cm, widths of 50 cm, and lengths of 25 cm. This research did not evaluate differences in regard to bank height because Chu-Agor *et al*. (2007) demonstrated that bank height only affects the initial stability of the bank, not the seepage erosion process. The bottom of the soil block was lined with a 2.5 cm densely packed clay layer to serve as a restrictive layer. The rest of the block was packed with soil to the desired ρ_b in 2.5 cm lifts. All soil was packed when the soil had reached near residual soil moisture content (i.e., 0.05 to 0.10 g water per g soil). The soil was then cut to simulate various bank angles, α (90^o, 75^o, and 60^o) such that the horizontal centerline for each bank remained 25 cm away from the water inlet. For the experiments, heads (H) of 15, 25, or 35 cm were maintained in the inflow reservoir using a Marriott-type infiltrometer.

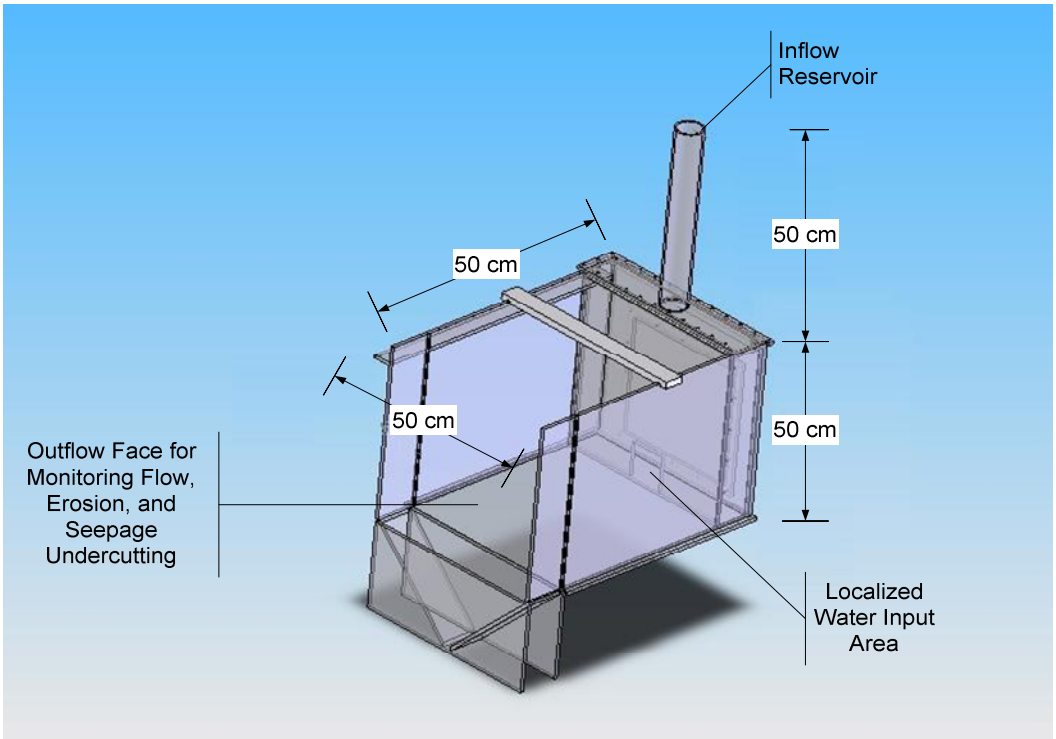

Figure 3-1. Three-dimensional soil box used to simulate seepage erosion of single-layer, repacked soil banks. The inflow reservoir is capable of producing seepage heads up to 100 cm.

Data collected during the experiments included the flow arrival time at the bank face, the time of seepage erosion initiation, seepage erosion as a function of time, and the volume of bank collapse. During the experiment, seepage erosion particle mobilization and undercutting were monitored over time using a three-dimensional laser scanner (3D Digital Corporation, Sandy Hook, CT). This laser scanner is a medium range scanning instrument with resolutions of 135 μm at a 300 mm scanning distance and 210 μm at a 650 mm scanning distance with a point density of 255 by 1000 points. For the laboratory experiments, all scans were captured within 650 mm of the bank face. Data from the 3-D scanner were used to investigate the hydraulic controls producing a given seepage erosion mechanism. Scanned images were exported to an ASCII file in terms of the rectilinear three-dimensional coordinates of the point cloud. The coordinates were then used to

create 2.0 mm square grids using the inverse to distance power algorithm. The eroded volume was computed by subtracting the scanned surface at a given time from the scanned surface of the initial bank. An example of the eroded surface by seepage particle mobilization is shown in Figure 3-2.

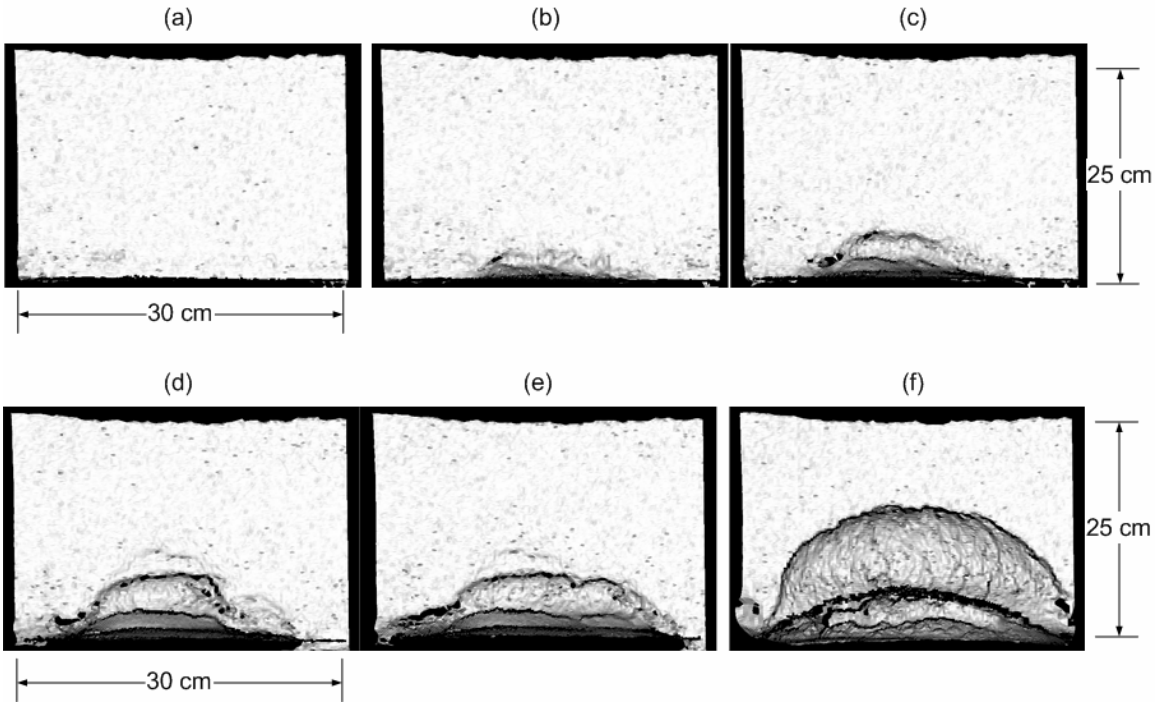

Figure 3-2. Example of the eroded surface by seepage particle mobilization captured using the three-dimensional laser scanner. Each scan represents a different time during the experiment: (a) original bank face, (b) and (c) illustrate the start of the seepage particle mobilization and undercutting, (d) and (e) illustrate continued undercut growth, and (f) illustrates the bank after small-scale sapping failure on the bank slope.

3.3.2 Trends in Seepage Undercutting

For cases with seepage particle mobilization and undercutting, the shape of the eroded surface was investigated for each of the seepage headcuts. A three-dimensional Gaussian function was fit to the data, given by:

$$z(x,y) = A\exp\left[-\left\{\left(\frac{x-x_o}{\sigma_x}\right)^2 + \left(\frac{y-y_o}{\sigma_y}\right)^2\right\}\right] \quad (9)$$

where $z(x,y)$ is the measured seepage headcut from the original bank face, A is the amplitude or maximum distance of seepage erosion, x_o and y_o are the center of the amplitude, and σ_x and σ_y are spreads of the seepage headcut. The spreads are related to the full width at half-maximum ($FWHM_j$) of the Gaussian function, where:

$$FWHM_j = 2\sqrt{2\ln(2)}\sigma_j \quad (10)$$

where j is either the x or y coordinate. Each image generated from the scanner was used to identify the initial mode of erosion: unimodal or multimodal. Unimodal erosion represents undercutting that is focused at a single point on the bank face whereas multimodal represents erosion that initiated at more than one location. With this data, trends were investigated between the depth and width of undercutting as functions of soil type, ρ_b, α, and H.

3.4 Results and Discussion

3.4.1 Characteristics of Seepage Erosion Undercutting

For cases where seepage undercutting occurred, the depth of undercutting required for a bank collapse was most dependent on the soil ρ_b as compared to α or H for these experimental conditions (Figure 3-3). The error bars shown in Figure 3-3 represent variability due to the imposed inflow H and α. For experiments with the same soil type, α and H, the required amplitude of undercutting (A), which generally fell within the range

of 2.0 to 7.0 cm, decreased as the ρ_b decreased (Table 3-1) due to the corresponding decrease in *c'*. Correspondingly, the cumulative volume of seepage erosion required to cause bank failure decreased as the ρ_b decreased (Table 3-1). The loamy sand soil generally required equivalent to slightly lower amplitudes of undercutting for bank collapse than the sand experiment based on experiments with the same ρ_b (i.e. 1.60 g cm^{-3}), α (90°, 75°, and 60°), and H (15, 25 and 35 cm). Therefore, sediment transport models for seepage erosion should include an explicit consideration for the ρ_b of the noncohesive sediment.

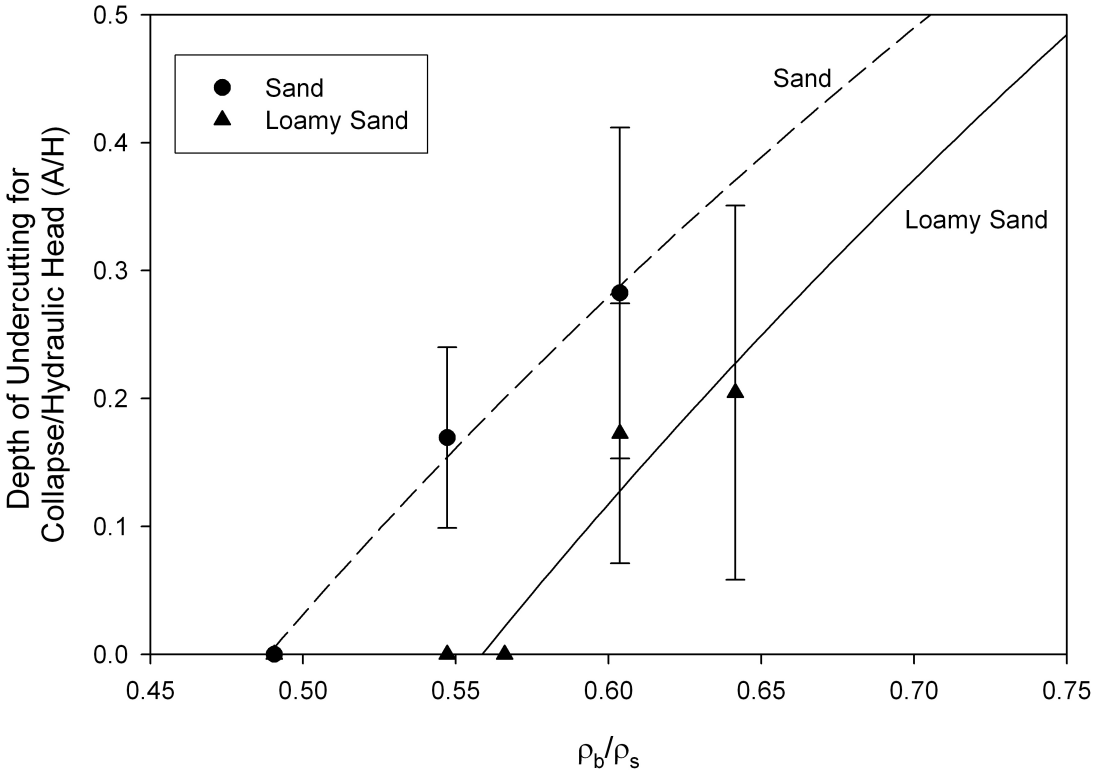

Figure 3-3. Relationship between maximum depth of undercutting (i.e., amplitude, *A*) required for a bank failure to the bulk density (ρ_b) non-dimensionalized by the particle density (ρ_s) of the soil. The symbols represent the averages relative to varying bank slope and water head for each soil type.

Table 3-1. Observed seepage erosion volume (V_{SE}), volume (V_{BF}) of soil loss by bank failure, and amplitude or maximum distance of undercutting (A) prior to bank collapse, relative to experimental soil block conditions (α is the bank angle, H is the inflow water reservoir head, and ρ_b is the soil bulk density). Values are averages of at least duplicate experiments.

		Sand				Loamy sand			
α	H	ρ_b	A	V_{SE}	V_{BF}	ρ_b	A	V_{SE}	V_{BF}
(^{o})	(cm)	(g cm^{-3})	(cm)	(cm^3)	(cm^3)	(g cm^{-3})	(cm)	(cm^3)	(cm^3)
90	15	1.60	4.9	592.1	6672.4	1.70	6.1	1448.7	6144.8
		1.45	4.9	475.0	6465.4	1.60	2.3	129.8	5235.2
		1.30	PO	PO	5727.2	1.50	PO	PO	4811.1
						1.45	PO	PO	6133.5
						1.30	PO	PO	4710.9
90	25	1.60	6.3	781.0	6353.7	1.70	3.0	221.0	3285.2
		1.45	4.2	252.0	6559.8	1.60	3.4	281.9	2974.9
90	35	1.60	4.3	183.2	6609.3	1.70	1.5	26.1	3806.6
		1.45	3.0	140.5	NA †	1.60	3.1	180.1	5573.8
75	15	1.60	6.2	867.3	4870.0	1.70	5.2	937.2	4665.7
		1.45	2.5	93.9	4184.5	1.60	3.4	305.1	4239.0
		1.30	PO	PO	NA				
75	25	1.60	6.2	799.6	5995.8	1.70	3.5	345.3	2856.1
		1.45	2.9	176.9	3324.8	1.60	3.6	333.0	3692.9
75	35	1.60	5.8	576.7	5790.9	1.70	2.8	216.0	3429.1
		1.45	2.8	142.6	2924.2	1.60	2.6	212.5	4408.6
60	15	1.60	6.5	1137.1	5842.3	1.70	6.7	1492.0	5347.6
		1.45	4.4	437.0	4713.3	1.60	6.2	846.2	4966.1
60	25	1.60	6.6	813.9	5081.7	1.70	3.8	306.2	3365.6
		1.45	6.0	744.4	5033.9	1.60	5.3	288.1	4117.1
60	35	1.60	5.6	508.0	4421.7	1.70	5.8	1191.0	4195.8
		1.45	7.0	197.8	5169.9	1.60	4.4	626.3	3650.0

*PO is tension or "pop-out" failure due to pore-water pressure gradient without seepage undercutting (and was not a topic of this paper).

†Data not collected during the experiment.

For experiments on the same soil with equivalent α and ρ_b, an increase in H generally resulted in less seepage erosion and correspondingly lower amplitudes required for bank failure (Table 3-1). The increased H theoretically resulted in greater soil pore-

water pressures in the overlying topsoil which reduced the shear strength of the soil. These results are consistent with Fox *et al*. (2006, 2007a, 2007b) and Wilson *et al*. (2007) in that seepage particle mobilization and increased soil pore-water pressure are both important processes leading to bank failures. As α decreased for a particular ρ_b and H, the amplitude of the seepage undercut required for bank collapse increased. This result is fundamentally obvious since lower α result in initially more stable banks (higher factor of safety), requiring a greater amplitude of seepage undercut to cause a failure (Chu-Agor *et al*., 2007).

3.4.2 Unimodal versus Multimodal Seepage Headcuts

For cases in which the seepage process was by seepage erosion undercutting, it was observed during the experiments that seepage erosion can initiate as a unimodal headcut, in which erosion is concentrated at one location on the bank face, or as a multimodal headcut, in which erosion initiates at different locations on the bank face. A typical time sequence demonstrating the changes in the seepage headcut as seepage erosion progresses is shown in Figure 3-4 for the case of a unimodal headcut. Also shown is the Gaussian fit for these specific headcuts. The strength of the fit, quantified through calculation of the coefficient of determination, or R^2, was greater in cases where the seepage erosion headcuts initiated at one location on the bank face.

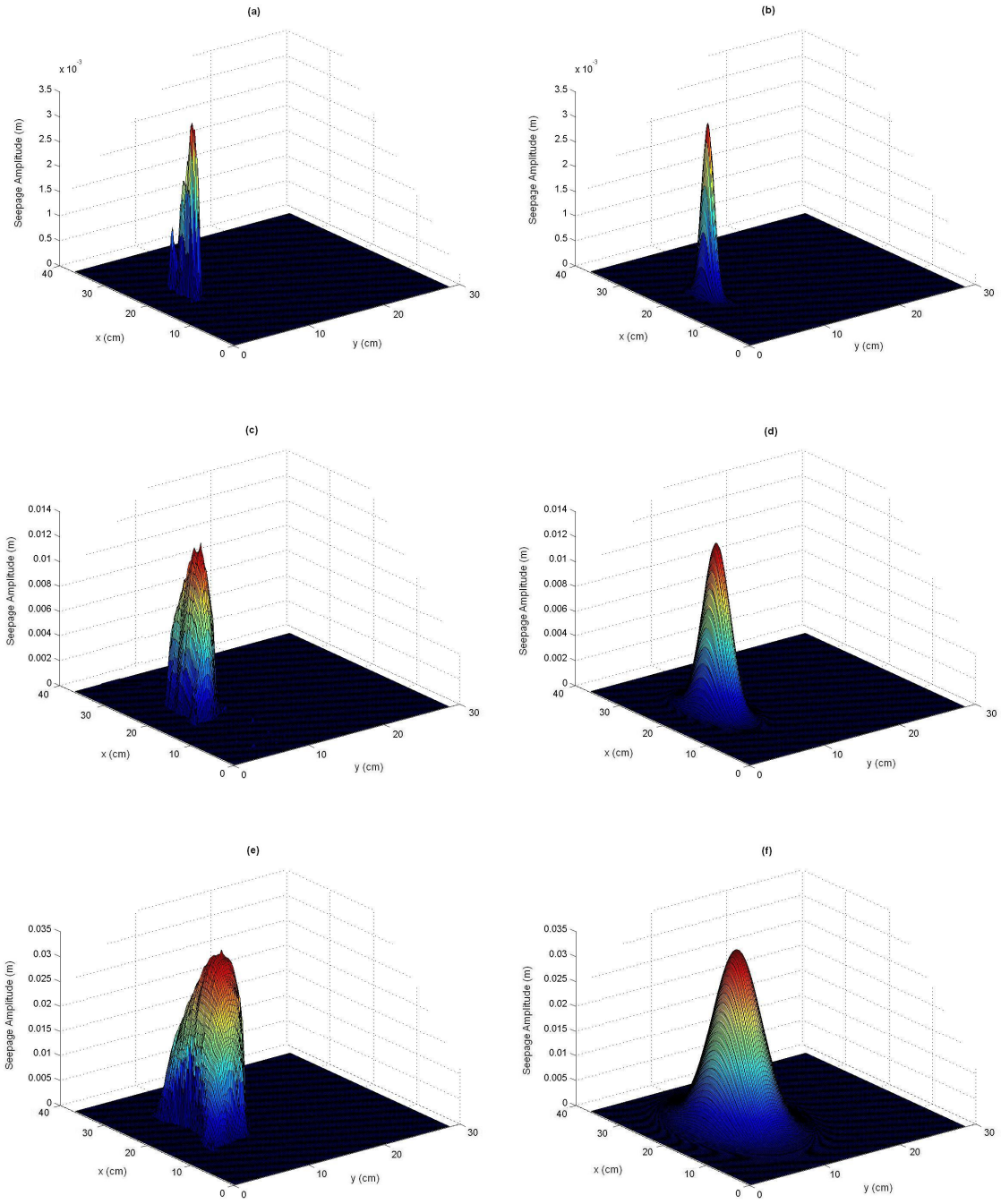

Figure 3-4. Typical time sequence of seepage erosion headcut formation. Note that the x-y plane is the bank face. Example shown is for the case of a 90° sand bank, 35 cm water head with ρ_b = 1.60 g cm^{-3}. (a) t = 108 s after flow arrival, (b) Gaussian fit for t = 108 s (R^2 = 0.80), (c) t = 125 s after flow arrival, (d) Gaussian fit for t = 125 s (R^2 = 0.77), (e) t = 149 s after flow arrival, and (f) Gaussian fit for t = 149 s (R^2 = 0.78).

It was hypothesized that multimodal headcuts would form in experiments with lower α, lower ρ_b, and lower inflow H. However, for these experimental conditions, the mode of initial seepage erosion undercutting was controlled by α. A 90^o bank, regardless of the H, ρ_b, and soil type, started with unimodal erosion, while banks with α of less than 90^o (i.e., 75^o and 60^o) started with multimodal erosion. The 90^o banks manifested in initial unimodal headcuts horizontally centered along the bank face, while the 75^o and 60^o banks started with multimodal headcuts that initiated at random locations within the seepage layer (Figure 3-5).

The multimodal headcuts generally converged into unimodal headcuts, with this convergence time hypothesized to depend on soil type, ρ_b, α, and inflow H. For α less than 90^o, convergence was identified from the scanned images and was verified using the regression coefficient from the Gaussian solid. An R^2 of at least 0.70 was used as an identifier for convergence. The time for the multimodal headcuts to converge to a concentrated unimodal erosion headcut was prominently controlled by the inflow H. The higher the H the less time it took for convergence to occur for both soil types at different ρ_b (Figure 3-6).

Contrary to initial hypotheses, convergence time was more dependent on α than ρ_b for the range of ρ_b investigated in this research. Convergence times as a function of H were approximately equal for the same soil with different ρ_b but the same α. Once converged, the resulting unimodal headcut possessed greater lateral spreads (i.e., larger σ_x), sometimes extending the entire width of the bank face.

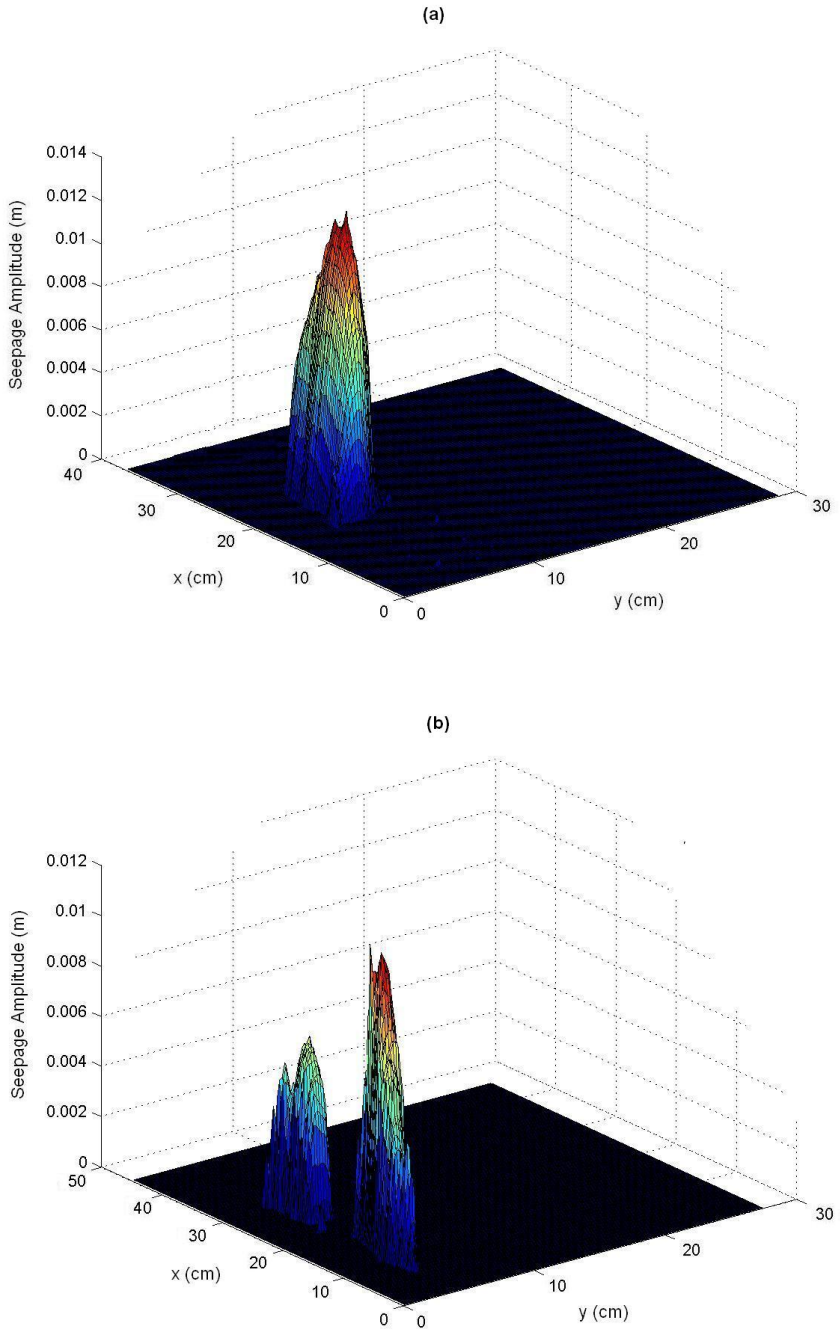

Figure 3-5. Example of (a) unimodal and (b) multimodal seepage erosion headcuts. Note that the x-y plane is the bank face. The unimodal figure is for the case of loamy sand with 90^{o} bank, 35 cm head, and 1.60 g cm^{-3} bulk density. The bimodal figure is for the loamy sand with 75^{o} bank, 15 cm head, and 1.70 g cm^{-3} bulk density.

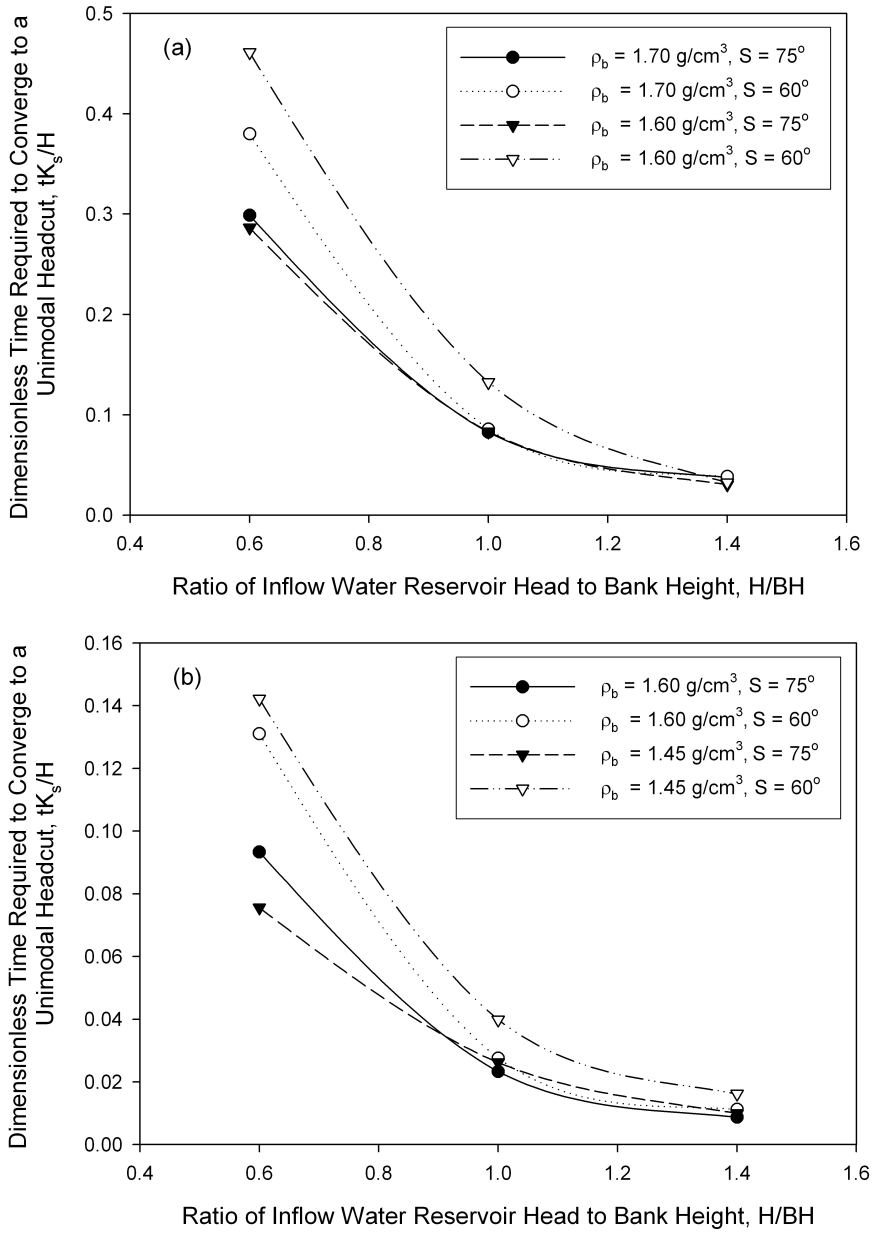

Figure 3-6. Time required for multimodal seepage particle mobilization headcuts for (a) sand and (b) loamy sand soils to reach unimodal headcut, non-dimensionalized by the saturated hydraulic conductivity, Ks, and the water inflow reservoir.

3.4.3 Trends in Undercut Shapes

For a given headcut amplitude (A), the width of the undercut (i.e., σ_x) was approximately an order of magnitude greater than the height (i.e., σ_y) of the undercut (Figure 3-7). Regression curves through the A-σ_y data demonstrated similar power-curve relationships for the sand and loamy sand soils. The A-σ_x relationships had greater scatter but still demonstrated a fairly uniform pattern between the two soil types. In fact, the sand soils typically followed a strong linear relationship before experiencing data scatter for $A > 4$ cm. The scatter from a linear trend line started at smaller A for the loamy sand soil (i.e., $A > 1$ cm). Differences in the A-σ_x relationships for the sand and loamy sand soils were less apparent at lower A. These common relationships were most likely functions of the similar c' (i.e., less than 7.5 kPa) and ϕ' (i.e., between 25^o and 40^o) between the two soils. No apparent dependency of the A-σ_y and A-σ_x relationships on ρ_b was observed. These results suggest that it may be possible to use such generalized relationships as a first approximation for inclusion of seepage particle mobilization and undercutting into stability models.

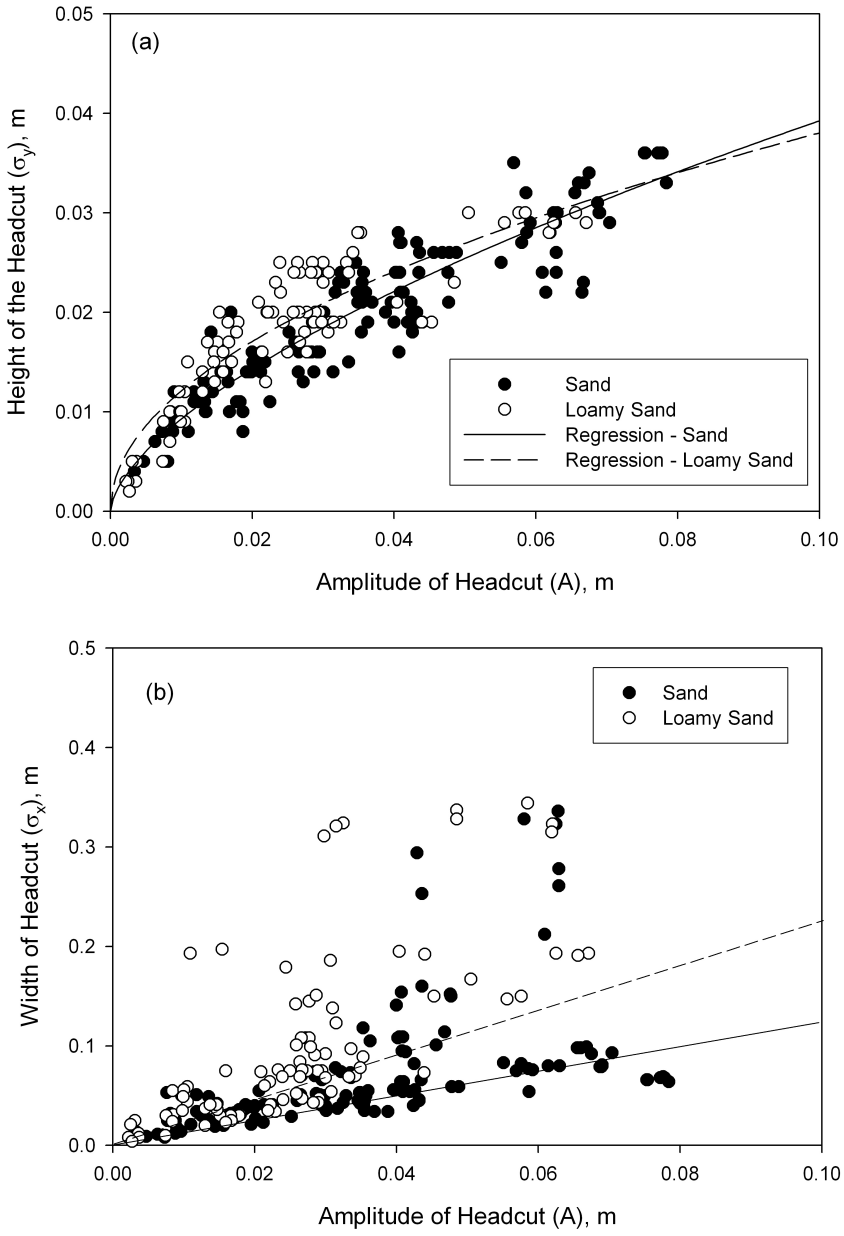

Figure 3-7. Observed relationship between the amplitude (*A*) of the headcut and the (a) height as quantified by the spread (i.e., σ_y) and (b) width of the headcut (σ_x) for the sand and loamy sand soils.

3.5 Summary and Conclusions

For banks experiencing seepage particle entrainment and undercutting, the slope of the bank predominately influences the undercutting formation. For these experimental conditions, unimodal headcuts were observed throughout the experiment for banks with 90^{o} slopes. On banks with smaller slopes, the headcuts generally initiated as multimodal, eventually converting to a unimodal headcut sometime before bank failure and controlled largely by the hydraulic gradient and the bulk density.

Relationships were developed between the amplitude, width, and height of the headcut for both the sand and loamy sand soils investigated in this research. A power law relationship was observed between amplitude and height with the relationship similar for both soils. Differences in soil type were more prevalent in the relationships between amplitude and width. However, the differences may not be significant so that these generalized relationships could be used to predict the width and height of the undercut based on *a priori* knowledge of the amplitude. The advantage of this fact is for the eventual incorporation of this seepage mechanism into stability models.

Even though there has been work on the effect of the change in the geometry of the bank due to undercutting on bank failure, such as the static analyses reported by Wilson *et al*. (2007) and the step-wise dynamic analysis by Chu-Agor *et al*. (2007), a fully integrated variably saturated flow model with a dynamic geometric and geotechnical model to predict bank failure is still lacking. Along with a sediment transport function capable of predicting the mass of seepage erosion, it may be possible in future research to relate this sediment mass to an amplitude of headcut and eventually to an estimate of the three-dimensional headcut structure.

CHAPTER IV

LABORATORY EXPERIMENTS OF THE INFLUENCE OF VEGETATION ON THREE-DIMENSIONAL SEEPAGE EROSION UNDERCUTTING

4.1 Abstract

Though root reinforcement plays a prominent role in streambank stability and there has been recent work analyzing the effects of *in situ* root reinforcement on soil shear strength, the number of controlled studies to quantify root reinforcement is limited. Four 50 cm cubic soil blocks, each with a focused inflow reservoir, were constructed to investigate the effects of vegetation on seepage erosion and streambank stability. Experiments included 25-cm tall, 90^{o} loamy sand banks packed at 1.6 g cm^{-3} bulk densities. A constant head of 25 cm was imposed on the soil to induce flow. Switchgrass (*Panicum virgatum*) was planted on top of three of the four soil blocks (one as control with bare soil) and was allowed a two-month growth period inside a greenhouse. A laser scanner was utilized to obtain the three-dimensional coordinates of the bank and undercut surfaces at approximately 15 to 30 s intervals. The stressed state of the vegetation yielded lower root reinforcement values (6.2 to 12.4 kPa) than *in situ* field measurements (i.e., 18 kPa). Soil blocks with greater root reinforcement experienced longer times to bank failure, up to a certain limit, than their counterparts with lower root cohesion values. The

seepage erosion undercutting patterns of these experiments also differed from previous experiments due to soil weathering. Separate stability analyses incorporating (1) seepage erosion undercutting and (2) seepage erosion forces confirmed the need for a conglomerate model with both destabilizing mechanisms for streambank stability predictions.

4.2 Introduction

The complex interaction between seepage and other failure and stability mechanisms makes it difficult to fully understand the role of seepage on hillslope, bank, and gully instability. According to Crosta and di Prisco (1999), in order to understand the onset of streambank instability due to seepage, it is important to point out that collapse is the final result of a complex chain of events due to the partial saturation of the materials, the three-dimensional geometry of the problem, and the heterogeneity of the materials. Budhu and Gobin (1996) studied slope instability due to ground-water seepage on unvegetated homogeneous soils at low slopes in order to provide bounds on the seepage direction that provokes slope failures. They concluded that hydraulic gradient and seepage direction are uniquely related at the seepage face and are not independent variables. They also showed that seepage direction that initiates static liquefaction depends on bank slope angle and soil unit weight.

Slope instability due to increased pore-water pressure brought about by seepage has been well documented to cause bank instability (Abam, 1993; Darby and Thorne, 1996; Crosta and di Prisco, 1999; Rinaldi and Casagli, 1999; Simon *et al*., 1999) and provided the core concepts of the Bank Stability and Toe Erosion Model (BSTEM)

developed by the USDA-ARS National Sedimentation Lab (Simon and Collison, 2002). Soil strength or the resisting force which is responsible for bank stability is defined by the Mohr-Coulomb equation:

$$\tau_f = c' + (\sigma - \mu_w)\tan\phi' \tag{4-1}$$

where τ_f is the shear stress at failure (kPa), c' is the effective cohesion (kPa), ϕ' is the effective angle of internal friction (degrees), σ is the total normal stress (kPa), and μ_w is the soil pore-water pressure (kPa) (Whitlow, 1983; Fredlund and Rahardjo, 1993). In unsaturated soils, increasing matric suction increases the apparent cohesion of the soil, as described by Fredlund and Rahardjo (1993):

$$\tau_f = c' + (\sigma - \mu_w)\tan\phi' + (\mu_a - \mu_w)\tan\phi^b \tag{4-2}$$

where μ_a is the soil pore-air pressure (kPa) and ϕ^b is the angle indicating the rate of increase in the shear strength relative to matric suction and is generally between 10^o and 20^o. Using this information, as well as user-defined geotechnical streambank parameters, BSTEM calculates the factor of safety (*FS*), which is a ratio of the resisting forces (τ_f) to the driving forces (matric suction depletion, etc.)

Pore-water pressure increases reduce the effective stress and shear strength of a soil. Seepage force, which is another destabilizing force, acts on grains of sediment and is proportional to the hydraulic gradient $\frac{\partial\psi}{\partial y}$ where ψ is the matric suction and y is a distance:

$$\tau_s = \rho g d \frac{\partial\psi}{\partial y} \tag{4-4}$$

where τ_s is the seepage stress (kPa), ρ is the density of the fluid (kg m^{-3}), g is gravity (m s^{-2}), and d is the grain diameter (m). Several studies have incorporated this seepage force into equations for particle mobilization by seepage such as Lobkovsky *et al*. (2004) who modified the Shields number to include this seepage force. Chu-Agor *et al*. (2008) also included seepage force in a *FS* equation for the failure plane parallel to the bank face:

$$FS = \frac{c' A' + \sigma' \tan \phi'}{W \sin \alpha + f_s \sin \lambda} \tag{4-5}$$

where *A'* is the sheared area, σ' is the effective normal force, W is the weight of the soil element, α is the bank angle, f_s is the seepage force on the element, and λ is the direction of the seepage vector measured clockwise from the inward normal to the bank slope. For the failure plane associated with the bank face, the effective normal force is:

$$\sigma' = W \cos \alpha - f_s \cos \lambda \tag{4-6}$$

where W and f_s are given by:

$$W = \gamma' V \tag{4-7}$$

$$f_s = i \gamma_w V \tag{4-8}$$

where i is the magnitude of the hydraulic gradient (i.e., $\sin \alpha / \sin \lambda$) and V is the volume of the soil element. They found that λ varied from 180^o to 270^o at the drainage face.

Research has also demonstrated that vegetation plays a role in bank stability, both advantageous and disadvantageous through root reinforcement, surcharge, and hydrologic influences, such as soil water uptake (Wu *et al*., 1979; Wu, 1984; Thorne, 1990; Beeson and Doyle, 1995; Gray and Sotir, 1996; Simon and Collison, 2002; Micheli and Kirchner, 2002; Pollen *et al*., 2004; Simon *et al*., 2006; Zaimes *et al*., 2006; Pollen, 2007). Small amounts of root reinforcement can provide substantial increases in soil shear strength

(Waldron, 1977; Wu *et al.*, 1988a, 1988b; Riestenberg, 1994). Pollen (2007) also noted that root reinforcement increased bank stability over a wide range of soil moisture conditions, but the magnitude varied as a function of soil shear strength and soil moisture content.

Since fibrous roots of vegetation are strong in tension, but weak in compression, their combined effects with soil (which is strong in compression, but weak in tension) create a fairly strong composite material (Wu *et al*., 1979; Wu, 1984; Thorne, 1990; Gray and Sotir, 1996; Micheli and Kirchner, 2002; Simon and Collison, 2002; Pollen *et al*., 2004; Simon *et al*., 2006; Pollen, 2007). Therefore, the tensile stabilizing forces of the roots were incorporated into BSTEM Version 4.1 via the Wu *et al*. (1979) equation:

$$c_r = T_r\left(A_r / A\right)\left(\cos\theta \tan\phi' + \sin\theta\right) \cong 1.2 T_r\left(A_r / A\right) \tag{4-3}$$

where c_r is the cohesion due to roots (kPa), T_r is the tensile strength of roots (kPa), A_r/A is the area of shear surface occupied by roots per unit area (root-area ratio), and θ is the shear distortion from vertical (degrees) (Waldron, 1977; Waldron and Dakessian, 1981). Tensile strengths of roots are typically measured through the application of a load to one end of a single root (Simon and Collison, 2002; Pollen and Simon, 2005; Pollen, 2007; Pollen *et al*., 2007).

Pollen and Simon (2005) recently made strides to increase the accuracy of root-reinforced streambank failure mechanisms. They suggest that while BSTEM Version 4.1 utilizes a perpendicular root reinforcement model which assumes that all of the tensile strength of the roots is mobilized instantaneously, in reality, roots within a given soil matrix have different tensile strengths and will break progressively, with an associated redistribution of the stress as each root breaks. This suggests that BSTEM is

overestimating the effect of vegetation on the mass stability of streambanks and that a fiber bundle model of root reinforcement should be included (Pollen and Simon, 2005; Pollen *et al*., 2007).

Pollen (2007) investigated the effects of root reinforcement with pore-water pressure variation on streambank stability. She found that while the tensile strength of roots was largely independent of soil moisture, the threshold diameter between root pullout and breaking decreases when pore-water pressure increases. This is due to decreasing frictional bonds between the roots and the soil with decreasing matric suction (Pollen, 2007).

While the processes associated with root reinforcement and streambank instability due to decreasing matric suction are better understood, this study tries to understand the impact of root reinforcement on seepage erosion via a controlled laboratory analysis. Pollen (2007) measured tensile and breaking forces of *in situ* roots and Tosi (2007) quantified the tensile strength of field-originating roots in a laboratory machine for the purpose of addressing slope stability; however, few, if any, controlled studies to quantify root reinforcement have ever been performed. Furthermore, no studies have investigated the interaction between seepage and vegetation.

4.3 Materials and Methods

4.3.1 Experimental Setup and Data Analysis

Four three-dimensional clear acrylic glass soil blocks with dimensions 50 cm by 50 cm by 50 cm (Figure 4-1) were constructed with two compartments: a focused water

reservoir (10 cm high by 10 cm wide centered at the bottom of the back face of the soil block) where a constant water head is maintained and the soil compartment which simulates a single layered hillslope, gully sidewall, or streambank. A loamy sand soil (85% sand, 13% silt, d_{50} = 0.24 mm) was packed to a bulk density (ρ_b) of 1.6 g cm^{-3} in all four soil blocks. The bottom of the soil blocks were lined with a 2.5 cm densely packed clay layer to serve as a restrictive layer. The rest of the blocks were packed at near residual soil moisture content (i.e., 0.05 to 0.10 g water per g soil) in 2.5 cm lifts. All experiments consisted of soil blocks with heights of 25 cm, widths of 50 cm, and lengths of 30 cm.

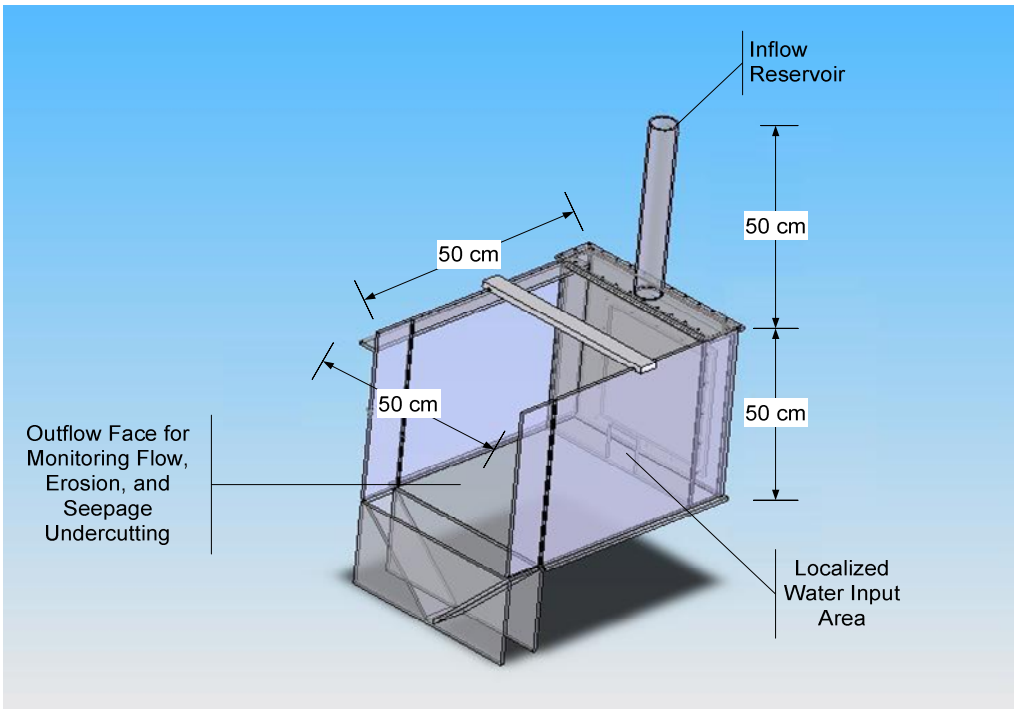

Figure 4-1. Three-dimensional soil box used to simulate seepage erosion of single-layer, repacked soil banks. The inflow reservoir is capable of producing seepage heads up to 100 cm.

Once three of the soil blocks were packed to 20 cm in height, 10 clusters (two to three stems connected to a single root mass) of switchgrass (*Panicum virgatum*), obtained

from the USDA-ARS National Sedimentation Lab in Oxford, Mississippi, were bare rooted and planted and the remaining 5 cm of soil were packed in two lifts around the stems. The switchgrass was planted in a random pattern within a 10 cm wide portion of the top of the bank, which was 5 cm from the bank face (Figure 4-2). The switchgrass was allowed two months (mid-November to mid-January) to establish and grow in the soil blocks. Each block, including a fourth control block without vegetation, was given an equivalent amount of water (i.e., approximately 1 L every 2 to 3 days) with MiracleGro® Liquid All Purpose Plant Food application every 14 days.

Following the two month growth period, the experiments were performed in the same fashion as those in Chu-Agor *et al*. (2008) with all banks at their original 90^{o} packing angle (α) and a constant head (H) of 25 cm in the inflow reservoir (using a Marriott-type infiltrometer). All of these vegetated soil block experiments, as well as the control experiment, were performed inside a greenhouse for increased viability of the switchgrass plants.

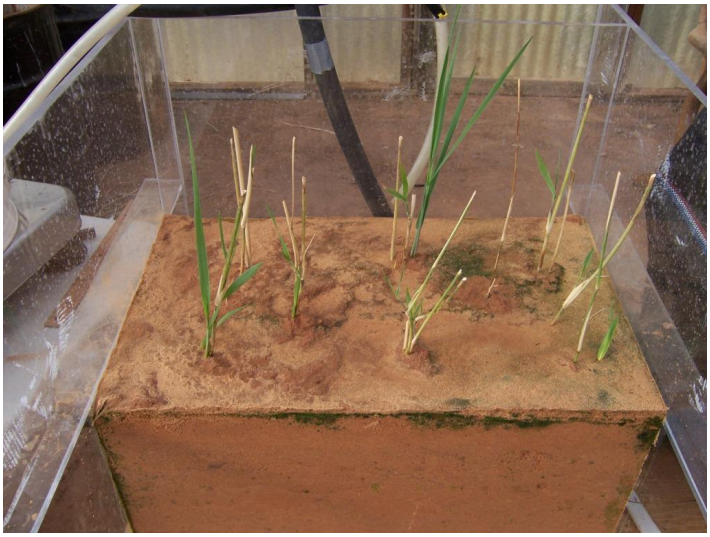

Figure 4-2. Switchgrass (*Panicum virgatum*) clusters were planted in a random pattern on the top of the bank face. All plants were within a 10 cm wide space which began 5 cm from the bank face. The plants were allowed to establish and grow in the soil block for two months inside a greenhouse.

Data collected during the experiments were similar to those collected in Chu-Agor *et al*. (2008), including the flow arrival time at the bank face, the time of seepage erosion initiation, the shape of seepage erosion with regard to root presence at the bank face, and the volume of bank collapse. During the experiment, seepage erosion was monitored over time using a three-dimensional laser scanner (3D Digital Corporation, Sandy Hook, CT). This laser scanner is a medium range scanning instrument with resolutions of 135 μm at a 300 mm scanning distance and 210 μm at a 650 mm scanning distance with a point density of 255 by 1000 points. For the laboratory experiments, all scans were captured within 650 mm of the bank face. Scanned images were exported to an ASCII file in terms of the rectilinear three-dimensional coordinates of the point cloud. The coordinates were then used to create 2.0 mm square grids using the inverse to distance power algorithm. The eroded volume was computed by subtracting the scanned surface at a given time from the scanned surface of the initial bank to estimate the shapes of seepage undercutting and root reinforcement characteristics.

Following the conclusion of seepage experiments, root characteristics were evaluated. Root area ratio (A_R/A) was determined by measuring the length and diameter of roots exposed on the failure plane with a standard metric ruler and calipers. The plants were then extracted from the failed soil block and the root tensile strength for all of the vegetation in each block was measured using an Instron® Universal Materials Testing Machine (www.instron.com) via the application of an upward 5 kN load until failure (Figure 4-3).

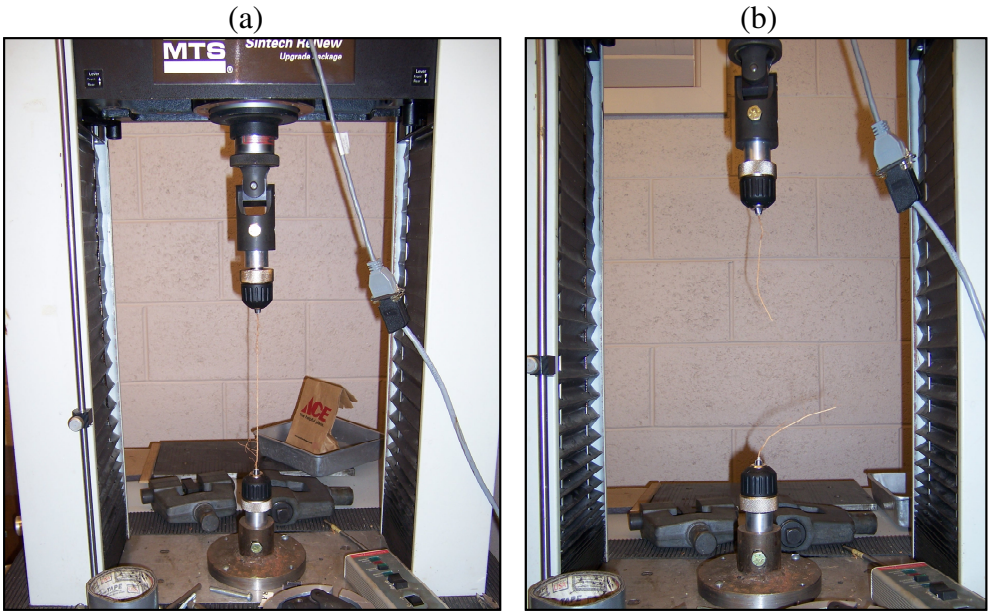

Figure 4-3. (a) Root tensile strength was measured through the application of an upward load until (b) failure in an Instron® Universal Materials Testing Machine.

4.3.2 Application of BSTEM and Stability Equations

The vegetated soil blocks were modeled in BSTEM as a single 22.5 cm layer bank above an extremely cohesive 2.5 cm clay layer with $\alpha = 90^{o}$. BSTEM is capable of simulating pore water pressure effects and seepage undercutting but not seepage forces. Various groundwater table depths were analyzed—at 100%, 60%, and 20% of the total bank height (*BH*). Various depths of undercutting (d_u), ranging from no undercutting (d_u = 0 cm) to d_u = 19 cm (the maximum allowable undercut depth of the noncohesive seepage layer based on the dimensions of the soil block profile and the shear surface angle, which is a function of φ' and α), were incorporated into BSTEM to try to simulate the instability and failure observed in the lab and to investigate the sensitivity of BSTEM to undercutting. In addition, c' values of 4.9 and 8.9 kPa (using a c_r value of 4.0 kPa

found from an average value of 8.0 kPa with a 50% vegetation safety margin, which is recommended by Pollen and Simon (2005) to account for overestimation of root cohesion by the Wu *et al*. (1979) equation) were used to model both unvegetated and vegetated soil blocks, respectively.

The *FS* values for the vegetated and control soil blocks were also determined using equation (4-5) derived by Chu-Agor *et al*. (2008). This equation does not model seepage undercutting but does consider seepage forces. The same *c'* values used in BSTEM simulations, as well as parameters of the soil and soil blocks were used. The *FS* was first calculated with this equation for instances when no seepage forces were present for comparison to BSTEM simulations. To simulate seepage forces, λ ranging from 185^{o} to 270^{o} were simulated, which is the possible range suggested by Chu-Agor *et al.* (2008).

4.4 Results and Discussion

4.4.1. Root Characteristics

Characteristics of the switchgrass roots along the failure plane varied between three-dimensional soil blocks. The tensile strength of the roots was determined for ranges of root diameters (Table 4-1). The average root diameter amongst all of the plants was 1.00 mm. The tensile strength values (T_r) found in these experiments are considerably less than *in situ* measurements of switchgrass taken by Simon and Collison (2002). They found switchgrass roots ranging from 0.1 to 4.7 mm in diameter with tensile strengths between 1.9 and 128 MPa. This difference may be due to stresses the plants experienced being grown outside of field conditions and during the dormant season. In this research,

the fully-grown plants were extracted from the Mississippi field site in mid-summer, potted in field soil, then bare-rooted and transplanted into the loamy sand in the soil blocks in November. Another factor affecting these strength values may be in the method of measurement between investigations. Simon and Collison (2002) utilized the same mechanism, identified as a Root Puller and developed by Abernethy and Rutherford (2000), as Pollen and Simon (2005) and Pollen (2007) for field-site measurements. For their *in situ* measurements, these authors dug trenches along the sides of streambanks, exposing roots along the bank profile. One end of the Root Puller was attached to a root and the other to a load cell. As the load cell increased tension on the root, breaking forces and pullout forces were measured, each of which varied with pore water pressure.

Table 4-1. Average tensile strength (T_r) associated with ranges of root diameter sizes (d).

d Range (mm)	Average T_r (MPa)
0.55-0.69	0.68
0.70-0.99	0.78
1.00-1.39	1.12
1.40-1.60	1.43

The increased cohesion due to roots (c_r) was calculated from equation (4-3) using A_R/A and T_r associated with both the average root diameter from all three soil blocks (Avg T_r) and the average diameter per block from listed diameter ranges in Table 4-2 (d range T_r). Though the root area ratios (A_R/A) in the soil blocks (0.0032 to 0.0092) were greater than those for switchgrass found *in situ* (0.00014) by Simon and Collison (2002), c_r values are, as expected, less than the 18 kPa found in the field. This is because c_r is also correlated to T_r (values of which are one to two orders of magnitude less than *in situ* values).

Table 4-2. Total root area (A_R), root area ratio (A_R/A), and increased soil cohesion due to roots (c_r) for each of the three-dimensional vegetated soil blocks. The c_r was found using both the tensile strength for the overall average root diameter (Avg T_r) and for the average diameter size (d_{avg}) in each soil block using the T_r for the range which that diameter falls into (d range T_r).

	A_R (cm^2)	A_R/A (%)	c_r (kPa) Avg T_r	d_{avg} (mm)	c_r (kPa) d range T_r
Vegetation 1	9.52	0.76	8.80	0.64	6.20
Vegetation 2	4.05	0. 32	3.74	1.08	4.36
Vegetation 3	11.48	0. 92	10.62	1.08	12.37

4.4.2 Characteristics of Seepage Erosion on Root Reinforced Soil Blocks

Though performed under the same hydraulic conditions ($\alpha = 90^o$, $\rho_b = 1.6$ g cm^{-3}, and $H = 25$ cm), an initial and obvious difference was noticed between the seepage erosion shapes of the control and vegetated soil blocks and those experiments in Chu-Agor *et al*. (2008). Concentrated unimodal headcuts formed during all 90^o bank simulations in Chu-Agor *et al*. (2008); however, multimodal formations occurred across the entire width of the bank face during these experiments (for all vegetated blocks as well as the control block). In addition, smaller amplitudes of undercutting (A) were required prior to bank collapse than in the Chu-Agor *et al*. (2008) experiments. This difference in seepage erosion phenomena can be explained by processes which may have occurred during the vegetation-establishing period. The excess time the soil spent in the blocks prior to induced heads, as well as the constant altering of soil moisture content (via the watering process), may have allowed weathering by means of both microbial activity and wetting and drying cycles. These weathering processes can increase cohesion and filter clay particles toward the bank face, thereby allowing full saturation of the bank prior to seepage flow and, correspondingly, larger seepage forces at the time of failure.

Even with smaller seepage erosion failure depths, noticeable differences occurred between not only the control and vegetated blocks, but also amongst the vegetated blocks themselves. These differences seem to be correlated with root area ratios on the failure plane (A_R/A) and increased cohesion due to roots (c_r). Greater values of the maximum amplitude of bank failure (A_{BF}) and total volume of bank collapse (V_{BF}) are associated with higher c_r values. Both banks with visible roots on the face experienced slower times to failure (t_{BF}) following the initiation of seepage flow at the face (Table 4-3). For these experiments, a direct correlation could not be found between c_r and A or V_{SE} as c' did (via increased bulk density, ρ_b) in the unvegetated banks of Chu-Agor *et al*. (2008); however, with experimental replication, this may be achieved.

Table 4-3. Seepage erosion volume (V_{SE}), volume (V_{BF}) of soil loss by bank failure, amplitude or maximum undercutting distance (A) prior to bank collapse, maximum amplitude of bank failure (A_{BF}), and time from seepage flow initiation to bank failure (t_{BF}) versus root cohesion (c_r) in the controlled vegetated soil block experiments.

	c_r (kPa)	A (cm)	V_{SE} (cm^3)	A_{BF} (cm)	V_{BF} (cm^3)	t_{BF} (min)
Vegetation 1	6.2	1.53	51.0	11.35	3819.4	5.52
Vegetation 2	4.4	1.30	19.8	8.05	3295.8	4.13
Vegetation 3	12.4	1.08	12.0	12.20	3093.6	5.47
Control	0.0	1.17	385.1	7.00	2300.0	3.20

Figure 4-4 shows the correlation between c_r and t_{BF}. As c_r increases, up until a certain value (i.e., approximately 6.0 kPa), the roots have a direct impact on bank stability which is represented by the increased time between seepage flow initiation and bank failure (t_{BF}). However, after a certain value of c_r, the increased cohesion from the roots does not further stabilize the bank and t_{BF} does not further increase. Pollen (2007) found a similar asymptotic relationship in her *in situ* studies, noting that root

reinforcement only increases soil shear strength to a certain value before it has no additional impact on soil shear strength.

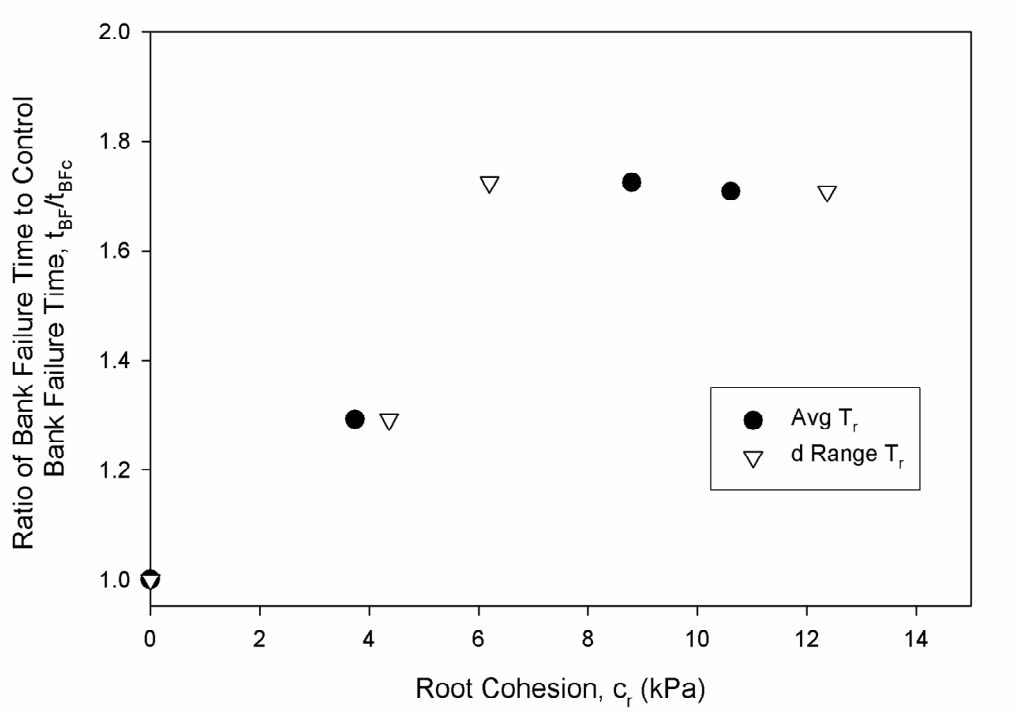

Figure 4-4. An increase in time from seepage flow initiation to bank collapse (t_{BF}) occurs with increasing cohesion due to roots (c_r) to a maximum t_{BF} at which further increases in c_r no longer influence t_{BF}. "Avg T_r" values correspond to the overall average root diameter and "*d* range T_r" corresponds to the average root diameter in individual soil blocks. Note that t_{BFc} corresponds to the control block.

The main factor affecting the shape and duration of seepage erosion undercutting is the presence of visible root structures, or lack thereof, on the bank face prior to inducing water heads on the soil blocks. The failure sequence of one of the two vegetated soil block with roots visible on the initial bank face is shown in Figure 4-5a. This figure shows how the shape of the undercut forms around the roots and the tensile strength of the roots hold the bank into place. When roots are not present on the initial bank face, as occurred in one of the vegetated soil blocks, the failure plane is not sufficiently reinforced and failure occurs more rapidly (Figure 4-5b). Figure 4-5 also demonstrates

the relatively shallow erosion amplitudes (1.08 to 1.53 cm in the vegetated blocks) noted earlier. Because these erosion shapes never became unimodal prior to bank failure, a Gaussian distribution for undercutting shape, like those found in Chu-Agor *et al.* (2008), can not be applied.

Figure 4-5. Failure sequence of a vegetated soil block (a) with visible roots on the initial bank face and (b) without visible roots on the initial bank face. As seepage occurs, the visible roots influence the shape of erosion; whereas, without visible roots seepage flow intersects the bank face freely and failure occurs more rapidly.

4.4.2 Stability Analysis of Vegetated Soil Blocks

All three root-reinforced soil blocks and the control block experienced failure after the build-up of pore-water pressure due to seepage, as well as shallow seepage undercutting. However, when modeled in BSTEM even with seepage undercutting, no *FS* values fell below the critical value for instability (*FS* = 1.0) (Figure 4-6). For the

undercutting depths and fully saturated conditions observed before failure in the vegetated soil blocks, BSTEM predicted a *FS* of 8.0 to 9.1. Since BSTEM allows the user to input undercutting but does not predict seepage force, this program did not calculate the instability and ultimate failure observed in the lab.

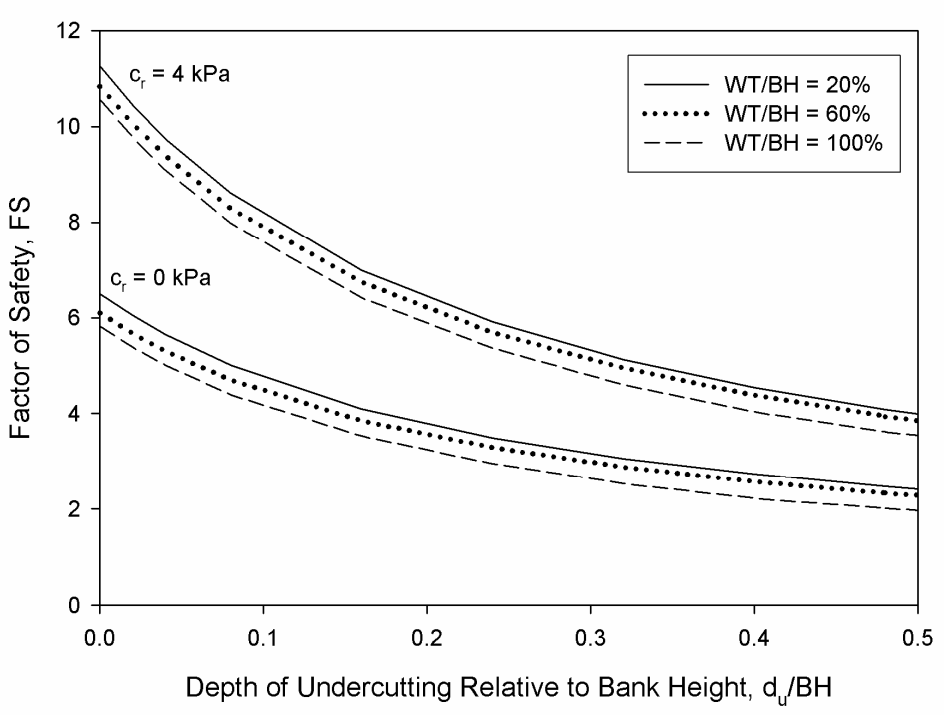

Figure 4-6. Stability analyses in BSTEM showed that all soil blocks, both vegetated and unvegetated, were always stable.

For no seepage forces or undercutting, the *FS* values predicted using equation (4-5) were almost identical (varying only 0.7 to 2%) to the *FS* simulations in BSTEM; however, the error increases (up to 6 to 8%) with decreasing matric suction in the bank (higher water table heights relative to *BH*) since equation (4-5) is only valid for unsaturated conditions and BSTEM performs a limit equilibrium analysis under both saturated and unsaturated conditions. With seepage forces, the *FS* was only found to be unstable (*FS* < 1.0) under one set of conditions: when $\lambda = 185^{o}$ (Figure 4-7). This is also

the smallest possible value for λ in which the equation remains valid. Chu-Agor *et al.* (2008) suggest a typical λ of 210^o, which results in a *FS* of 6.8 when using a *c'* of 8.9 kPa.

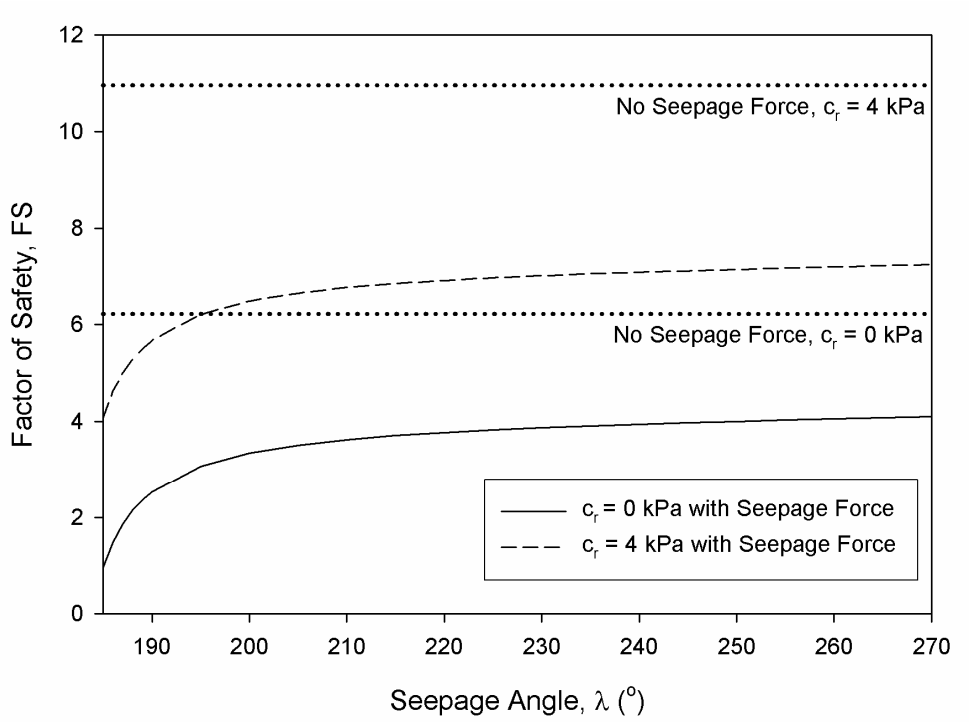

Figure 4-7. *FS* calculated using Chu-Agor et al. (2008) equation for various angles of the seepage vector (λ).

Neither BSTEM nor equation (4-5) derived by Chu-Agor *et al.* (2008) suggested instability and failure as demonstrated in the vegetated and control blocks in the laboratory. Since the current version of BSTEM can only account for undercutting and equation (4-5) can only simulate the seepage force, it becomes obvious that both destabilizing forces are needed in a *FS* calculation to properly analyze the complex nature of streambank stability under conditions of active groundwater processes.

4.5 Summary and Conclusions

Laboratory root reinforcement values obtained during this investigation were considerably less than those found *in situ* by previous authors due to the smaller root diameters found in the soil blocks. This can be explained by both the stress experienced by the switchgrass being outside of field conditions with measurements taken during the dormant period, as well as use of different measurement methods between field and laboratory conditions.

Though performed under the same hydraulic conditions ($\alpha = 90^{o}$, $\rho_b = 1.6$ g cm^{-3}, and $H = 25$ cm), the seepage erosion and undercutting pattern of these vegetated soil blocks was distinct from the unvegetated soil block experiments reported by Chu-Agor *et al*. (2008). Due to excess time the soil spent in the blocks prior to induced seepage flow, as well as the constant altering of soil moisture content (via the watering process), weathering by means of both microbial activity and wetting and drying cycles were allowed to occur.

The vegetated and control soil blocks did not experience the unimodal undercutting like their unvegetated counterparts, but, rather, shallow multimodal cuts formed along the entire width of the bank face with visible root structures controlling the undercut shapes. Stability analyses revealed that neither BSTEM nor the equation derived in Chu-Agor *et al*. (2008) could predict instability in the simulated streambanks; therefore, these methods should be combined such that both seepage undercutting and seepage forces can be simulated. In future work, these vegetated soil block experiments should be repeated with greater vegetation density during the active growing season.

CHAPTER V

CONCLUSIONS AND FUTURE WORK

The factor of safety, *FS*, describes the inherent stability of a streambank and theoretically predicts the occurrence of streambank failure. The *FS* is most dependent on bank angle (α), bank height (*BH*), soil pore water pressure (μ_w), effective cohesion (c'), effective angle internal friction (φ'), bulk density (ρ_b), cohesion due to roots (c_r), seepage erosion undercutting (d_u), and seepage force (f_s). *FS* decreases with increasing α, μ_w, ρ_b, d_u, and f_s. Greater c_r values, however, result in higher *FS* values since they add to the soil effective cohesion (c').

The three-dimensional soil block investigations confirmed these notions about streambank stability in a controlled environment, even with the soil weathering processes that occurred during the vegetated soil block experiments. In the unvegetated soil block experiments, decreasing α consistently resulted in the need for greater depths of undercutting before bank failure would occur. At the same time, greater induced water heads (H) created a greater f_s and increased the rate at which μ_w built up, both of which resulted in shorter times to bank failure. When vegetation was added, the block with the least amount of root reinforcement and the control block also failed sooner than blocks reinforced with vegetation and higher c_r values.

Seepage erosion and undercutting formation varied in laboratory experiments with and without vegetation. The unimodal headcut shape, noted and described by a three-dimensional Gaussian distribution, common upon seepage erosion initiation to all of the 90^{o} blocks and after convergence of the multimodal headcuts of the lower bank angles in the unvegetated experiments, did not transfer, as hypothesized, to the vegetated soil block experiments. The 90^{o} vegetated banks instead experienced shallow, multimodal undercutting prior to bank failure by pore water pressure build up due to unexpected soil weathering processes. Further analyses of the vegetated experiments should be considered to confirm the effects of these weathering processes. For example, should the switchgrass be planted prior to its active season (i.e., April or May) and, therefore, only need two to four weeks for effective root growth, would these weathering processes still occur and alter the seepage headcut shape so dramatically?

In addition, future vegetated experiments should be performed under greater root densities (i.e., 20 to 30 or more switchgrass clusters, rather than the 10 used in these experiments) to analyze the full impact of root area ratios and root cohesion on the headcut shape and time to bank failure. To reduce the error associated with measurement methods, tensile strength data collected in future vegetated investigations should be performed with the same root-pulling device used in Pollen (2007). Further root-reinforced analyses may hopefully reveal generalized relationships, like those of the unvegetated blocks, which can be used to predict seepage headcut architecture on vegetated banks and hillslopes. Since most previous studies measured the effects of root reinforcement in field environments with multiple destabilizing forces, researchers could only attempt to roughly estimate root cohesion based on observed bank failures.

However, in the laboratory three-dimensional soil block experiments, the force (e.g., seepage erosion) exerted on the simulated streambanks was observed. Therefore, future vegetated soil block experiments will provide the controlled quantification of the effects of root reinforcement on seepage erosion and streambank stability and offer a significant contribution towards more effective river restoration engineering practices.

Both the Bank Stability and Toe Erosion Model (BSTEM), which can account for seepage undercutting but not seepage force, and the equation derived in Chu-Agor *et al*. (2008), which simulates the effects of seepage force but not undercutting, did not predict instability in the vegetated soil block experiments. Even though bank failure occurred in all root reinforced experiments, both models predicted FS values well over that of instability (FS = 1.0), ranging from 4.1 to 7.2 depending on seepage force angle (λ) in the Chu-Agor *et al.* (2008) equation and FS = 11.0 in BSTEM simulation. Therefore, future work should include the incorporation of both seepage undercutting and seepage force into a fully integrated dynamic streambank stability model that can predict the mass and headcut amplitude of seepage erosion and quantify the effects of root reinforcement on headcut formation to fully estimate three-dimensional headcut structures. Such a model, along with further understanding of the influences of root reinforcement on seepage erosion, would allow environmental and hydraulic engineers practicing in the river restoration field more accurate predictions of streambank instability, which will ultimately aid in the reduction of bank sediment losses and watershed pollution and decrease property damage from flooding associated with changes in stream flow regimes.

REFERENCES

Abam TKS. 1993. Factors affecting distribution of instability of river banks in the Niger delta. *Engineering Geology* 35: 123-133.

Abernethy B, Rutherfurd ID. 2000. The effect of riparian tree roots on the mass-stability of riverbanks. *Earth Surface Processes and Landforms* 25(9): 921-937.

ASCE Task Committee on Hydraulics, Bank Mechanics, and Modeling of River Width Adjustment. 1998. River width adjustment. I: Processes and mechanisms. *Journal of Hydraulic Engineering* 124(9): 881-902.

Barker DH. 1986. Enhancement of slope stability by vegetation. *Ground Engineering* 19 (3): 11-15.

Beeson CE, Doyle PF. 1995. Comparison of bank erosion at vegetated and non-vegetated channel bends. *Water Resources Bulletin* 31: 983-990.

Bradford JM, Piest RF. 1977. Gully wall stability in loess derived alluvium. *Soil Science Society of America Journal* 41(1): 115-122.

Budhu M, Gobin R. 1996. Slope stability from ground-water seepage. *Journal of Hydraulic Engineering* 122(7): 415-417.

Bull LJ, Kirkby MJ. 1997. Magnitude and variation in the contribution of bank erosion to the suspended sediment load of the River Severn, UK. *Earth Surface Processes and Landforms* 22(12): 1109-1123.

Burckhardt JC, Todd BL. 1998. Riparian forest effect on lateral stream channel migration in the glacial till plains. *Journal of the American Water Resources Association* 34: 179-184.

Byne WF. 2000. Predicting Sediment Detachment and Channel Scour in the Process-Based Planning Model ANSWERS- 2000. ME Thesis. Virginia Tech: Blacksburg, VA.

Chu-Agor ML, Wilson GV, Fox GA. 2007. Numerical modeling of bank instability by groundwater seepage flow. ASABE Paper No. 072117, American Society of Agricultural and Biological Engineers: St. Joseph, MI.

Chu-Agor M, Cancienne R, Fox GA, Wilson GV. 2008. Seepage mechanisms of hillslope, gully, and bank failure: Tension failure and three-dimensional seepage erosion undercutting. *Journal of Hydrology* (In review).

Coates DR. 1990. The relation of subsurface water to downslope movement and failure. In *Groundwater geomorphology: the role of subsurface water in earth-surface processes and landforms*, Higgins CG, Coates DR (eds). Geological Society of America: Boulder, CO; 51-76.

Crosta G, di Prisco C. 1999. On slope instability induced by seepage erosion. *Canadian Journal of Geotechnical Engineering* 36: 1056-1073.

Darby SE, Thorne CR. 1996. Numerical simulation of widening and bed deformation of straight sand-bed rivers. I. Model development. *Journal of Hydraulic Engineering* 122: 184-193.

Darby SE, Rinaldi M, Dapporto S. 2007. Coupled simulations of fluvial erosion and mass wasting for cohesive river banks. *Journal of Geophysical Research.* 112: F03022, doi: 10.1029/2006JF000722.

De Vries PG. 1974. Multi-stage line intersect sampling. *Forest Science* 20(2): 129-133.

Dunne T. 1990. Hydrology, mechanics, and geomorphic implications or erosion by subsurface flow. In *Groundwater Geomorphology: The Role of Subsurface Water in Earth-Surface Processes and Landforms*, Higgins CG, Coates DR (eds). Geological Society of America: Boulder, CO.

Evans DJ, Gibson CE, Rossell RS. 2006. Sediment loads and sources in heavily modified Irish catchments: A move towards informed management strategies. *Geomorphology* 79(1-2): 93-113.

Faulkner H. 2006. Piping hazard on collapsible and dispersive soils in Europe. In: *Soil Erosion in Europe*. J. Boardman and J. Poesen (eds.), John Wiley and Sons, Inc.: West Sussex, England.

Fox GA, Wilson GV, Periketi RK, Cullum RF. 2006. Sediment transport model for seepage erosion of streambank sediment. *Journal of Hydrologic Engineering* 11(6): 603-611.

Fox GA, Wilson GV, Simon A, Langendoen EJ, Akay O, Fuchs JW. 2007a. Measuring streambank erosion due to ground water seepage: correlation to bank pore water pressure, precipitation and stream stage. *Earth Surface Processes and Landforms* 32: 1558-1573.

Fox GA, Chu-Agor M, Wilson GV. 2007b. Erosion of noncohesive sediment by groundwater seepage flow: experiments and numerical modeling. *Soil Science Society of America Journal* 71(6): 1822-1830.

Fox GA, Chu-Agor ML, Wilson GV. 2007c. Seepage Erosion: A significant mechanism of stream bank failure. In *Proceedings of the World Water and Environmental Resources Congress 2007*, May 15-19, Tampa, FL, Kabbes KC (ed.). 243 (40927): 350.

Fredlund DG, Rahardjo H. 1993. *Soil Mechanics for Unsaturated Soils*. John Wiley and Sons: New York.

Gray DH, Sotir RB. 1996. *Biotechnical and Soil Bioengineering Slope Stabilization: A Practical Guide for Erosion Control*. John Wiley and Sons: New York.

Hagerty DJ. 1991a. Piping/sapping erosion. 1. Basic considerations. *Journal of Hydraulic Engineering* 117(8): 991-1008.

Hagerty DJ. 1991b. Piping/sapping erosion. 2. Identification/diagnosis. *Journal of Hydraulic Engineering* 117(8): 1009-1025.

Hey RD, Thorne CR. 1986 Stable channels with mobile gravel beds. *Journal of Hydraulic Engineering* 112: 671-689.

Hey RD, Heritage GL, Tovey NK, Boar RR, Grant N, Turner RK. 1991. *Streambank Protection in England and Wales* R&D Note 22, National Rivers Authority, London, 75 pp.

Higgins CG. 1982. Drainage systems developed by sapping on Earth and Mars. *Geology Boulder* 10(3): 147-152.

Higgins CG. 1984. Piping and sapping: development of landforms by groundwater outflow. In *Groundwater as a Geomorphic Agent,* LaFleur RG (ed). Allen and Unwin, Inc.: Boston, MA; 18-58.

Hooke JM. 1979. An analysis of the processes of river bank erosion. *Journal of Hydrology* 42: 39-62.

Howard AD, McLane, III CF. 1988. Erosion of cohesionless sediment by ground water seepage. *Water Resources Research* 24(10): 1659-1674.

Huang HQ, Nanson GC. 1997. Vegetation and channel variation: a case study of four small streams in southeastern Australia. *Geomorphology* 18: 237-249.

Jones JAA. 1997. Subsurface flow and subsurface erosion. In *Process and Form in Geomorpology*, D.R. Stoddart (ed). Routledge: London.

Laity JE. 1983. Diagentic controls on groundwater sapping and valley formation, Colorado Plateau, revealed by optical and electron microscopy. *Physical Geography* 4: 103-125.

Langendoen EJ, Lowrance RR, Williams RG, Pollen N, Simon A. 2005. Modeling the impact of riparian buffer systems on bank stability of an incised stream. In *Proceedings of the World Water and Environmental Resources Congress 2004*, May 15-19, Anchorage, AK, Walton R (ed.), DOI: 10.1061/40792.

Lindow N. 2007. *Channel Evolution of a Restored Low Gradient, Sand Bed Stream*. Ph.D. Dissertation, North Carolina State University, Raleigh, NC.

Lobkovsky AE, Jensen B, Kudrolli A, Rothman DH. 2004. Threshold phenomena in erosion driven by subsurface flow. *Journal of Geophysical Research-Earth Surface* 109(F4), Art. No. F04010.

Maher MH, Gray DH. 1990. Static response of sands reinforced with randomly distributed fibers. *Journal of Geotechnical Engineering* 116(11): 1661-1677.

McLane CF. 1984. *An Experimental and Theoretical Study of Seepage-Induced Erosion in Non-Cohesive Sediments*. Ph.D. Dissertation, University of Virginia.

McWhorter DB, Sunada DK. 1977. *Ground-Water Hydrology and Hydraulics*. Water Resources Publications, Highland Park, Colorado.

Micheli ER, Kirchner JW. 2002. Effects of wet meadow riparian vegetation on streambank erosion: Measurements of vegetated bank strength and consequences for failure mechanics. *Earth Surface Processes and Landforms* 27(7): 687-697.

Pollen N, Simon A, Collison A. 2004. Advances in assessing the mechanical and hydrologic effects of riparian vegetation on streambank stability. In *Riparian Vegetation and Fluvial Geomorphology*, Bennett SJ, Simon A (eds). American Geophysical Union: Washington, DC: 125-140.

Pollen N, Simon A. 2005. Estimating the mechanical effects of riparian vegetation on stream bank stability using a fiber bundle model. *Water Resources Research* 41, W07025, doi: 10.1029/2004WR003801.

Pollen N. 2007. Temporal and spatial variability in root reinforcement of streambanks: Accounting for soil shear strength and moisture. *Catena* 69(3): 197-205.

Pollen N, Simon A, Langendoen E. 2007. Enhancements of a bank-stability and toe-erosion model and the addition of improved mechanical root-reinforcement algorithms. In *Proceedings of the World Water and Environmental Resources Congress 2007*, May 15-19, Tampa, FL, Kabbes KC (ed.).

Riestenberg MM. 1994. Anchoring of thin colluvium by roots of sugar maple and white ash on hillslopes in Cincinnati. U.S. Geological Survey (USGS) Bulletin 2059-E, U.S. Government Printing Office: Washington, D.C.

Rinaldi M, Casagli N. 1999. Stability of streambanks formed in partially saturated soils and effects of negative pore water pressures: The Siene River (Italy). *Geomorphology* 26: 253-277.

Rowntree KM, Dollar ESJ. 1999. Vegetation controls on channel stability in the Bell River, Eastern Cape, South Africa. *Earth Surface Processes and Landforms* 24: 127-134.

Sekely AC, Mulla DJ, Bauer DW. 2002. Streambank slumping and its contribution to the phosphorus and suspended sediment loads of the Blue Earth River, Minnesota. *Journal of Soil and Water Conservation.* 57(5): 243-250.

Simon A, Curini A, Darby SE, Langendoen EJ. 1999. Streambank mechanics and the role of bank and near-bank processes in incised channels. In: *Incised River Channels*. Darby SE, Simon A (Eds), John Wiley and Sons, Chichester, UK, pp. 193-217.

Simon A, Darby SE. 1999. The nature and significance of incised river channels. In *Incised River Channels: Processes, Forms, Engineering and Management*, Darby SE, Simon A (eds). John Wiley and Sons: Chichester, UK, pp. 1-18.

Simon A, Curini A, Darby SE, Langendoen EJ. 2000. Bank and near bank processes in an incised channel. *Geomorphology.* 35(3-4): 193-217

Simon A, Collison AJC. 2002. Quantifying the mechanical and hydrologic effects of riparian vegetation on streambank stability. *Earth Surface Processes and Landforms* 27: 527-546.

Simon A, Pollen N, Langendoen E. 2006. Influence of two woody riparian species on critical conditions for streambank stability: Upper Truckee River, California. *Journal of the American Water Resources Association* 42(1): 99-113.

Simon A, Wells RR. 2006. Study of the effects of lateral seepage forces on tension-crack development, bank-failure dimensions and migration of edge of field gullies. In *Proceedings of the 8th Federal Interagency Sedimentation Conference*, April 2-6, 2006, Reno, Nevada.

Simon A, Pollen N, Jaeger K, Wohl E. 2007. Implications for the Removal of Invasive Species in Canyon de Chelly National Monument. In *Proceedings of the World Water and Environmental Resources Congress 2007*, May 15-19, Tampa, FL, Kabbes KC (ed.).

Stofleth JM, Shields FD, Fox GA. 2007. Hyporheic and total transient storage in small, sand-bed streams. *Hydrological Processes* DOI: 10.1002/hyp.6773.

Sultan N, Cochonat P, Canals M, Cattaneo A, Dennielou B, Haflidason H, Laberg JS, Long D, Mienert J, Trincardi F, Urgeles R, Vorren TO, Wilson C. 2004. Triggering mechanisms of slope instability processes and sediment failures on continental margins: a geotechnical approach. *Marine Geology* 213: 291-321.

Thorne CR. 1990. Effects of vegetation on riverbank erosion and stability. In *Vegetation and Erosion*, Thornes JB (ed). John Wiley and Sons: Chichester, UK; 125-144.

Tosi M. 2007. Root tensile strength relationships and their slope stability implications of three shrub species in the Northern Apennines (Italy). *Geomorphology* 87: 268-283

Trimble SW. 1997. Stream channel erosion and change resulting from riparian forests. *Geology* 25: 467-469.

van De Weil MJ, Darby SE. 2007. A new model to analyze the impact of woody riparian vegetation on the geotechnical stability of riverbanks. *Earth Surface Processes and Landforms* 32: 2185-2198.

Waldron LJ. 1977. The shear resistance of root-permeated homogeneous and stratified soil. *Soil Science Society of America Journal* 41: 843-849.

Waldron LJ, Dakessian S. 1981. Soil reinforcement by roots: Calculation of increased soil shear resistance from root properties. *Soil Science* 132(6): 427-435.

Whitlow R. 1983. *Basic Soil Mechanics*. Construction Press, New York.

Wilson GV, Jardine PM, Luxmore RJ, Zelazny LW, Lietzke DA, Todd DE. 1991. Hydrogeochemistry processes controlling subsurface transport from an upper subcatchment of Walker Branch watershed during storm events: 1. Hydrologic transport processes. *Journal of Hydrogeology* 123(3-4): 297-316.

Wilson GV, Periketi RK, Fox GA, Dabney SM, Shields FD, Cullum RF. 2007. Soil properties controlling seepage erosion contributions to streambank failure. *Earth Surface Processes and Landforms* 32: 447-459.

Worman A. 1993. Seepage-induced mass-wasting in coarse soil slopes. *Journal of Hydraulic Engineering* 119(10): 1155-1168.

Wu TH, McKinnell WP, Swanston DN. 1979. Strength of tree roots and landslides in Prince of Wales Island, Alaska. *Canadian Geotechnical Journal* 16(1): 19-33.

Wu TH. 1984. Effect of vegetation on slope stability. *Transportation Research Record* 965: 37-46.

Wu TH, Macomber RM, Erb RT, Beal PE. 1988a. Study of soil-root interactions. *Journal of Geotechnical Engineering* 114(GT12): 1351-1375.

Wu TH, Beal PE, Lan C. 1988b. In-situ shear test of soil-roots systems. *Journal of Geotechnical Engineering* 114(GT12): 1376-1394.

Wynn TM, Mostaghimi S, Burger JA, Harpold AA, Henderson MB, Henry LA. 2004. Variation in root density along stream banks. *Journal of Environmental Quality* 33(6): 2030-2039.

Wynn TM, Mostaghimi S. 2006. Effects of riparian vegetation on stream bank subaerial processes in southwestern Virginia, USA. *Earth Surface Processes and Landforms* 31(4): 399-413.

Zaimes GN, Schultz RC, Isenhart TM. 2006. Riparian land uses and precipitation influences on stream bank erosion in central Iowa. *Journal of the American Water Resources Association* 42(1): 83-97.

VITA

Rachel Michelle Cancienne

Candidate for the Degree of

Master of Science

Thesis: STABILITY OF ROOT REINFORCED STREAMBANKS: NUMERICAL MODELING AND LABORATORY EXPERIMENTS

Major Field: Biosystems and Agricultural Engineering

Biographical:

Personal Data: Born in New Orleans, Louisiana; the daughter of Gary and Maureen Cancienne.

Education: Received Bachelor of Science degree in Biosystems and Agricultural Engineering from Oklahoma State University, Stillwater, Oklahoma in December 2006. Completed the requirements for the Master of Science in Biosystems and Agricultural Engineering at Oklahoma State University in May, 2008.

Experience: Employed with Oklahoma State University, Department of Mathematics as an undergraduate, 2003 to 2006; employed as a National Science Foundation Research Experience for Undergraduates Intern during summer of 2006; employed with Oklahoma State University, Department of Biosystems and Agricultural Engineering as both a Graduate Research Assistant and Graduate Teaching Assistant, 2007 to present.

Professional Memberships: American Society of Agricultural and Biological Engineers.

Name: Rachel Michelle Cancienne Date of Degree: May, 2008

Institution: Oklahoma State University Location: Stillwater, Oklahoma

Title of Study: STABILITY OF ROOT REINFORCED STREAMBANKS: NUMERICAL MODELING AND LABORATORY EXPERIMENTS

Pages in Study: 85 Candidate for the Degree of Master of Science

Major Field: Biosystems and Agricultural Engineering

Scope and Method of Study: The scope of this study includes the effects of vegetation and root reinforcement on seepage erosion and undercutting as they regard streambank stability. An in-depth analysis of the effects of vegetation used in a current streambank stability software package, the Bank Stability and Toe Erosion Model, developed by the USDA-ARS National Sedimentation Laboratory was performed on previously studied streambanks. Laboratory experiments were then performed in a three-dimensional soil block in which steady heads were induced to cause subsurface flow events and seepage out of the simulated bank face. The laboratory experiments were performed with and without switchgrass (*Panicum virgatum*), after which the shape and properties of the seepage undercutting were analyzed.

Findings and Conclusions: The Bank Stability and Toe Erosion Model revealed, as expected, significant increases in streambank stability when all forms of vegetation were added to the streambank; however, this software is more significantly influenced by pore-water pressure distribution than root cohesion and seepage undercutting. Undercut formations of the seepage blocks varied between the unvegetated and vegetated three-dimensional soil block experiments. This can be explained by soil weathering patterns which may have occurred over the vegetation growth period; however, future replications of the vegetation experiments should be performed for a more in-depth analysis. Modeling of the vegetated soil block experiments revealed the need for the incorporation of both seepage undercutting and seepage force in future streambank stability software.

ADVISER'S APPROVAL: Dr. Garey A. Fox